Geophysical Journal International

Geophys. J. Int. (2015) **203,** 2070–2088 doi: 10.1093/gji/ggv426
GJI Geodynamics and tectonics

Large-scale gravity anomaly in northern Norway: tectonic implications of shallow or deep source depth and a possible conjugate in northeast Greenland

Sofie Gradmann[1] and Jörg Ebbing[1,2]

[1] *Geological Survey of Norway,* 7491 *Trondheim, Norway. E-mail: Sofie.Gradmann@NGU.NO*
[2] *Department of Geophysics, Christian-Albrechts-Universität Kiel, D-*24118 *Kiel, Germany*

Accepted 2015 September 30. Received 2015 September 30; in original form 2015 February 18

SUMMARY

A prominent gravity and geoid low lies just south of the Lofoten peninsula in northern Norway, partly coinciding with the location of Proterozoic granites of the Transscandinavian Igneous Belt and being offset by *ca*. 100 km to the highest topography of northern Norway. The study area extends both onshore and offshore and lies at the transition between Archaean and Proterozoic lithosphere. The Palaeoproterozoic basement has been overthrusted by the Palaeozoic nappes of the Caledonian orogen and now forms the passive margin of the NE Atlantic. We investigate the gravity anomaly performing combined 3-D geophysical-petrological forward modelling of the lithosphere and sublithospheric upper mantle using the interactive modelling program LitMod3D. We include variations in thickness and composition of the lithospheric mantle in order to include the effects on the rifted margin adjoining the Baltic craton. We compare three possible origins of the anomaly: (i) a low-density upper crust, representing the northward extension of the Transscandinavian Igneous Belt, (ii) a lower crustal source formed by a Moho depression and (iii) a thick, depleted lithospheric mantle of possibly Archaean origin. A similar, yet wider and stronger gravity anomaly is found on the conjugate margin in northeastern Greenland. A shallow crustal source is most consistent with the geophysical data sets. A respective source of the granitic belt, however, is difficult to reconcile with the regional geology both in Fennoscandia and Greenland. An additional contribution form a deeper source is suggested.

Key words: Gravity anomalies and Earth structure; Composition of the continental crust; Composition of the mantle; Cratons; Dynamics: gravity and tectonics.

1 INTRODUCTION

A prominent gravity low is situated in northern Norway (Fig. 1), which extends over 100 × 150 km and reaches negative values of −80 mGal in the free-air gravity and −130 mGal in the Bouguer gravity. Its presence has commonly been attributed to low-density granites of the Transscandinavian Igneous Belt (TIB). This igneous belt extends from southern Sweden, where it is exposed as granitic bedrock, to northern Norway (Fig. 2). Here it is primarily mapped by magnetic data and limited outcrops point towards granitoid rock types (Olesen *et al.* 2002; Skilbrei *et al.* 2002; Gorbatchev 2004; Olesen *et al.* 2010). However, the immediate correlation of the igneous rocks and the gravity low can be contested when additional geological and geophysical data sets are taken into account: The gravity response elsewhere along the TIB is much lower than at the northern Norwegian anomaly (NN anomaly). In addition, the isostatic response of a thick granitoid body is not consistent with the topography that is relatively low across the western part of the anomaly but rises to heights of 1500 m *ca.* 100 km east of the free-air gravity minimum (Fig. 3). Similarly, a very thick layer of TIB-like granitic rocks is poorly compatible with relatively low heat flow values indicated for this region (Pascal *et al.* 2007; Slagstad *et al.* 2009). In addition to that, the conjugate margin in northeast Greenland shows a strikingly similar gravity anomaly, thus with a larger extent and magnitude. There, the geological structures are substantially different than in Norway.

In this paper, we discuss different possible origins of the northern Norway gravity low, which could stem from sources located between the near-surface and the upper mantle. A wealth of available geophysical data sets is employed and different geological settings and tectonic processes are considered. Seismic and heat flow data are sparse in this region and simple forward models cannot be constrained accurately. We therefore test a number of different end-member scenarios using an integrated geophysical-petrological 3-D modelling approach in order to make use of the available information simultaneously and to reveal the implications and trade-offs between the data sets.

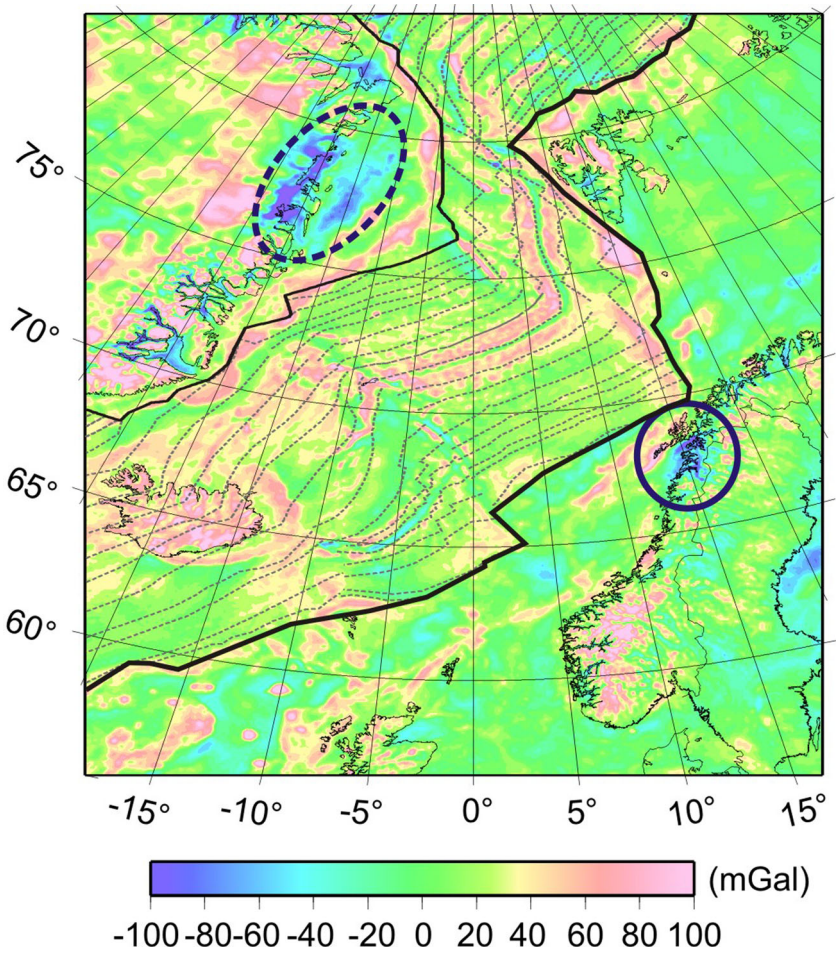

Figure 1. Free-air anomaly map of the north Atlantic. The prominent gravity anomaly in northern Norway is marked by a dark blue circle. A similar gravity anomaly is seen in northeast Greenland. Isochrones are shown as grey lines (Seton *et al.* 2012). Gravity data are taken from DTU2010 (Andersen 2010).

1.1 Background

1.1.1 Geology of Fennoscandia

Fennoscandia constitutes the westernmost part of the East European Craton and encompasses crustal domains of Archaean, Proterozoic and Phanerozoic tectonothermal ages (Fig. 2). The Archaean craton extends across northern Finland and northern Sweden into Norway (Gaal & Gorbatschev 1987; Lahtinen *et al.* 2005). The Palaeoproterozoic crust of southern Finland, Sweden and northern Norway was formed by large-scale terrane accretion and arc magmatism during the Svecofennian orogeny (2.1–1.8 Ga ago, Gorbatschev & Bogdanova 1993; Bingen *et al.* 2005; Lahtinen *et al.* 2005). At the end of the orogeny (1.86–1.65 Ga ago), the TIB was emplaced at the edge of the Svecofennian domain (Patchett *et al.* 1987; Gorbatschev & Bogdanova 1993). TIB is a collective term for a *ca*. 1400 km long roughly north–south trending batholith belt, partly covered by Caledonian rocks. Suggested emplacement mechanisms vary from an extensional intra-continental setting (Korja *et al.* 1993; Anderson 1997) to a continent-scale eastward subduction zone (e.g. Åhäll & Larson 2000; Lahtinen *et al.* 2009). The latter interpretation has recently been more favoured.

The terranes of the Sveconorwegian Province (also called Southwest Scandinavian Domain) were formed and modified during the Gothian (1.75–1.55 Ga) and the Sveconorwegian-Grenvillian orogeny (1.14–0.9 Ga, e.g. Gorbatschev & Bogdanova 1993; Bingen *et al.* 2005). It is not clear whether allochthonous terranes were accreted or existing terranes were re-organized (Bingen *et al.* 2008). The strongest deformation occurred in the region around and to the west of today's Oslo Graben, diminishing towards the north. Gradmann *et al.* (2013) employed 3-D lithospheric modelling to show that the Sveconorwegian Province comprises much thinner and compositionally heavier (less depleted) lithospheric mantle than the Palaeoproterozoic Baltic Shield. The boundary between the two mantle types occurs along a roughly N–S trending, narrow transition zone partly located under the Oslo Graben as is clearly imaged with *P*-wave tomography (Medhus *et al.* 2009). The surface transition from Sveconorwegian to Svecofennian crust, however, is mapped much further to the east in Sweden.

During the Caledonian orogeny (440–410 Ma ago) collisions with Laurentia (Greenland) in the west and Avalonia in the south affected the margin of Baltica. Allochthonous nappes of the Caledonides are still overlying the Proterozoic basement in Norway and Sweden and form the bulk part of the Scandinavian Mountain Chain. Along the southern margin of Baltica, orogenic remnants are no longer present at the surface, but crustal and upper-mantle structures reveal a major scar along the Trans-European Suture Zone. It extends from the East European platform into the North Sea (MONA LISA Working Group 1997a,b; Shomali *et al.* 2006). A northern branch, the Sorgenfrei-Tornquist Zone, extends from south of Norway, across Denmark into southernmost Sweden (Arlitt *et al.* 1999; Cotte *et al.* 2002; Plomerová *et al.* 2002; Shomali *et al.* 2002, 2006).

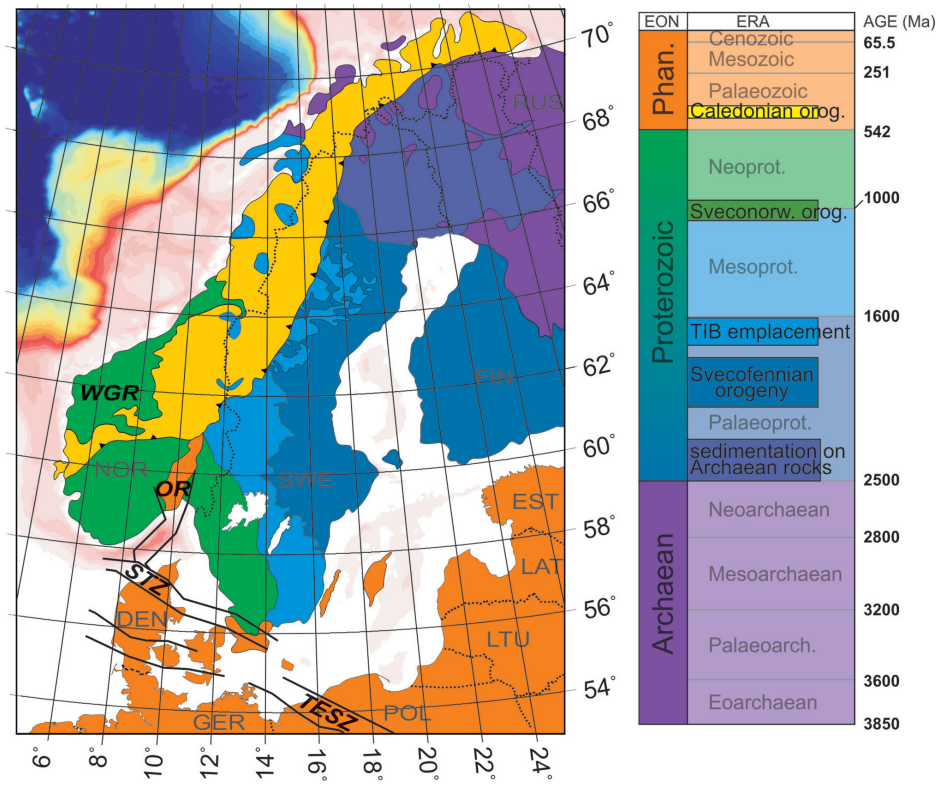

Figure 2. Simplified surface geological map of northern Europe and geological timescale showing relevant Fennoscandian tectonic events. The offshore regions display bathymetry from 0 to 1500 m water depth. WGR: Western Gneiss Region, OR: Oslo Rift, STZ: Sorgenfrei-Tornquist Zone, TESZ: Trans-European Suture Zone, TIB: Transscandinavian Igneous belt (modified after Gorbatchev 2004; Eken *et al.* 2008).

The Caledonian Mountains were lowered by orogenic collapse soon after collision and during a number of subsequent extensional phases. During the Permian, the Oslo Rift formed as a narrow extensional feature with localized magmatic activity. Widespread extension during the Late Jurassic to Early Cretaceous caused substantial thinning of the crust in today's shelf areas (Færseth & Lien 2002; Osmundsen *et al.* 2002). Rifting of the pre-thinned crust during the earliest Eocene led to the break-up of the Atlantic Ocean and was the last tectonic event in the Fennoscandian region.

1.1.2 Crustal and lithospheric structures of southern and northern Norway

The gravity anomalies shown in Fig. 3 indicate isostatic compensation over a large part of the Scandinavian mountains, because the free-air anomaly is close to zero and the prominent negative Bouguer anomaly traces the high topography. The Bouguer gravity low also extends into Sweden, where topography is not high, but granites of the TIB are present. These are generally, but not everywhere,

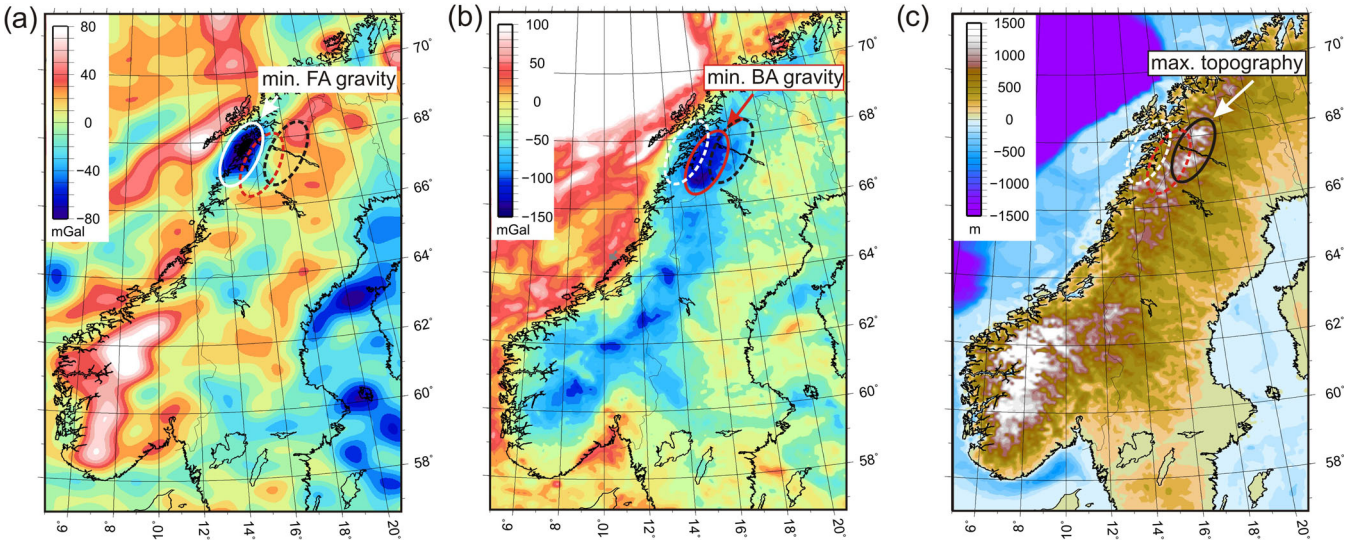

Figure 3. (a) Free-air gravity anomaly of western Fennoscandia. (b) Bouguer gravity anomaly of western Fennoscandia. Gravity data are taken from EGM2008 (Pavlis *et al.* 2008). (c) Topography of western Fennoscandia.

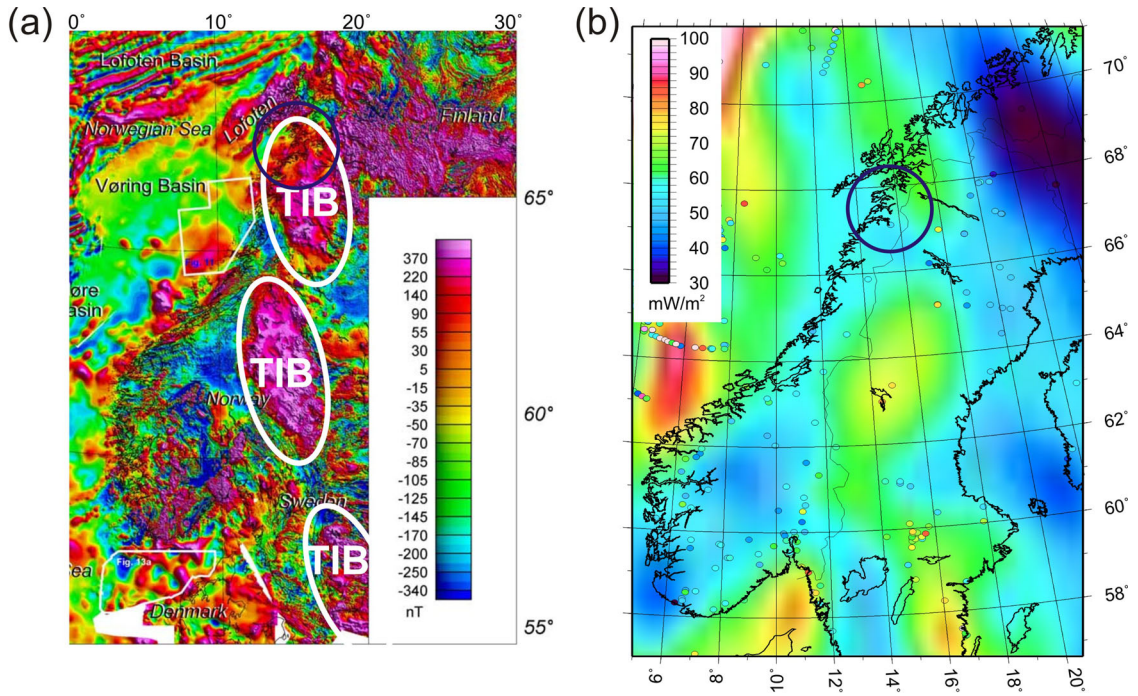

Figure 4. (a) Total magnetic field of western Fennoscandia (from Olesen *et al.* 2010). (b) Heat flow anomaly of western Fennoscandia showing interpolated data set and local, measured values (from Slagstad *et al.* 2009). Blue circle marks the location of the NN anomaly.

characterized by low density, high magnetic susceptibility and high heat production rates, which should make it easy to outline the TIB on gravimetric, magnetic and heat flow maps (Fig. 4). A small number of rock samples from the TIB show low magnetic susceptibility or low heat production. Gravity modelling constraines the thickness of the low-density TIB-like rocks in central Norway and Sweden to *ca*. 20 km (Skilbrei *et al.* 2002), heat flow modelling limits it to 12 km (Pascal *et al.* 2007), and isostatic modelling does not constrain it further (Ebbing 2007). In northern Norway, however, the geophysical data sets show a less consistent picture. The gravity values of the NN anomaly are much lower than elsewhere along the Scandinavian Mountain Chain or the TIB and are offset to the highest topography by up to 100 km (50 km for the Bouguer anomaly). Isostatic ratios between gravity and topography reveal that the northern gravity low has to be sourced at shallower depth than the gravity anomalies in southern Norway (Olesen *et al.* 2002; Ebbing & Olesen 2005). This conclusion is partly a result of the steep gradient at the flank of the gravity low. Areas of high magnetic anomalies can be related to the TIB but also to Archaean crust (Fig. 4).

Geoid and gravity gradients, which are more sensitive to structures at larger scales and larger depths, show distinct differences between southern and northern Fennoscandia. Both data sets show lows in northern Norway, whereas southern Norway with its higher topography is represented by positive values (Fig. 5). This now indicates a deep source of the anomaly especially since gravity gradients are not very sensitive to upper crustal structures (Ebbing *et al.* 2014). In addition, NE Greenland exhibits a similar yet wider and stronger anomaly that requires a source that is even larger in depth and/or extent.

Tomographic studies show an anomalously low velocity in the upper mantle under southern Norway (Medhus *et al.* 2009, 2012), which indicates a relatively warm (and thin) lithosphere. In addition to the relative abrupt change in lithosphere thickness, a change in its composition is also needed to satisfy the gravity and elevation data (Gradmann *et al.* 2013). This lateral variation in the subcontinental lithospheric mantle (SCLM) can be explained by the different tectonothermal ages (Phanerozoic-Neoproterozoic Sveconorwegian domain vs. Palaeoproterozoic Svecofennian domain). These ages control the degree of depletion of the lithospheric mantle and hence its chemical composition. In addition to the SCLM, the lower crust is distinctly different: a high-density lower crustal layer (LCL) is present in Finland and Sweden but tapers out under the high topography of the Scandinavian Mountain Chain (Ebbing 2007).

2 POSSIBLE EXPLANATIONS OF THE NN GRAVITY LOW

A shallow crustal source has most commonly been inferred as a source for the gravity low in northern Norway (Olesen *et al.* 2002), but cases can also be made for sources of intermediate to large depth. We discuss four different scenarios in the context of the geophysical data and geological constraints. These address the horizons or regions with major density contrasts as the most likely contributors to the gravity anomaly. Subsequently, we quantify the three most likely scenarios with 3-D forward models.

2.1 Scenario A: upper crustal structure

The gravity anomaly exhibits fairly steep flanks, which indicates a shallow source (Fig. 6). This and the low-density characteristics of granitoids suggest the TIB as a likely source. Geological mapping and magnetic anomalies both confirm the presence of the TIB in this region.

Models by Olesen *et al.* (2002) have shown that such low-density rocks must be up to 20 km thick in order to explain the gravity low. This might have large effects on heat flow and buoyancy and is not

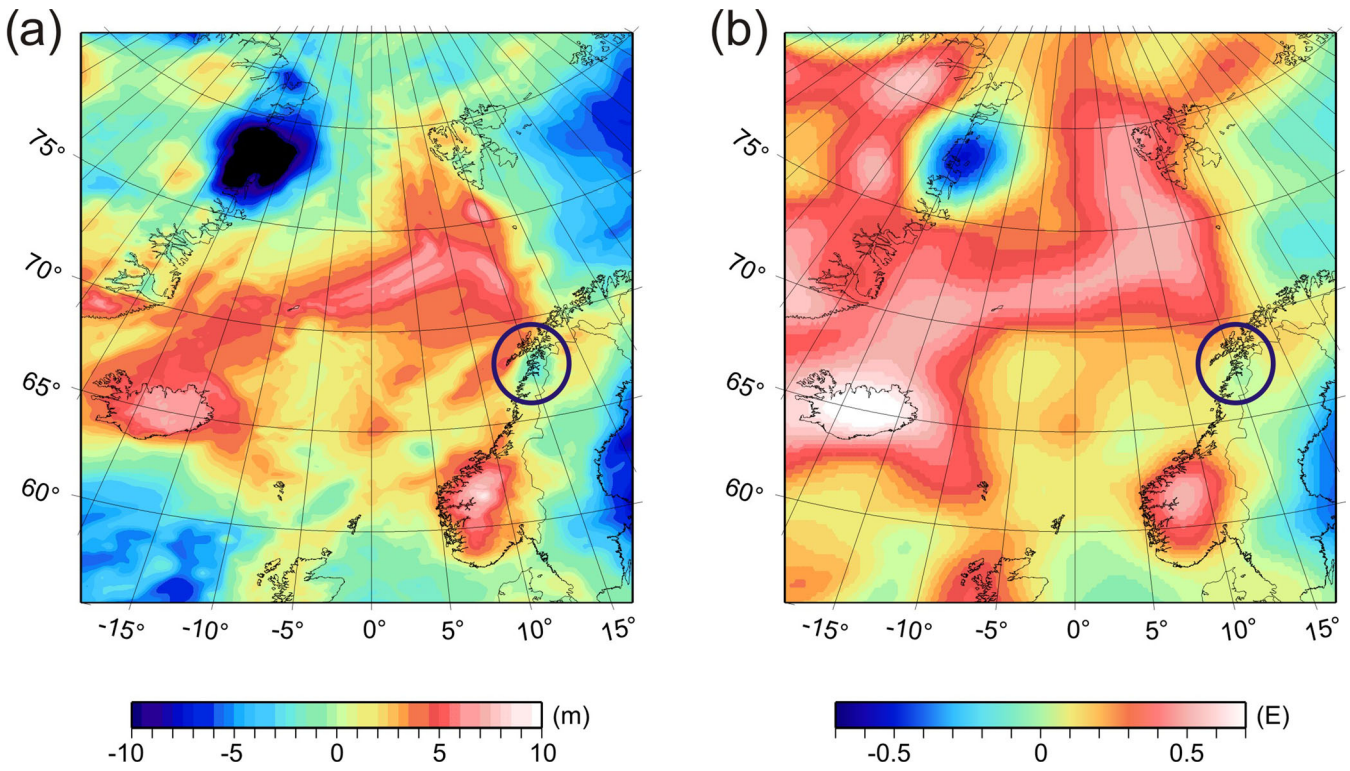

Figure 5. (a) Geoid of the north Atlantic region, filtered to degree and order 10 (EGM2008, Pavlis *et al.* 2012). (b) Vertical gravity gradient of the north Atlantic region measured at 255 km satellite height. Data from ESA satellite mission GOCE, http://www.goce4interior.dgfi.badw.de. Blue circle marks the location of the NN anomaly.

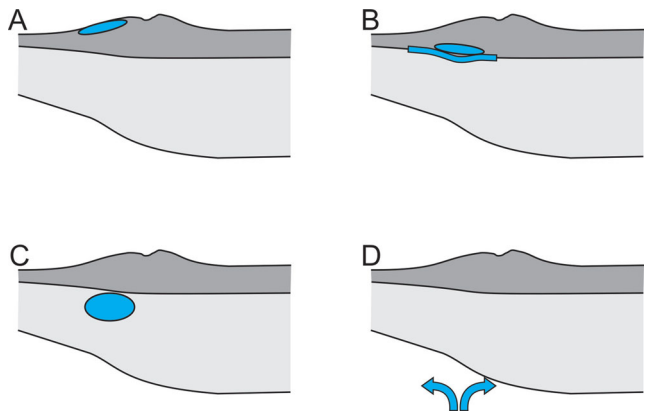

Figure 6. Possible scenarios to explain the gravity low with sources at different depth: scenario A, near-surface structure; scenario B, lower crustal structure; scenario C, uppermost mantle structure; scenario D, dynamic mantle effects.

easy to reconcile with the respective observations. Where the TIB is present elsewhere in Fennoscandia (Fig. 2), the gravity response is much lower than at the NN anomaly (Fig. 3). This is in spite of the overall lower-density granitic composition of the southern TIB rocks.

The conjugate margin in NE Greenland shows a somewhat similar, isolated gravity anomaly. However, no TIB-like granites or granitoids have been mapped here. The shape of the Greenland gravity low is large and semi-circular, not belt-like as it would be expected for a TIB-like structure.

2.2 Scenario B: lower crustal structure (LCL and Moho)

A high-density lower crust can be found throughout the Fennoscandian Shield (Henkel *et al.* 1990; Luosto 1997; England & Ebbing 2012). A non-uniform distribution of this layer—especially a local absence of the LCL—could generate a local gravity low (Fig. 6). The overall spatial distribution of the LCL, which has been estimated with isostatic modelling (Ebbing 2007), shows that this layer is already relatively thin along the entire Atlantic Norwegian coast. This limits the possible gravity effect that thickness variations might have.

A gravity low may stem from a Moho deepening, in other words from a crustal root. This has not been reported from seismic data, but deep refraction data are sparse and old in this region (Artemieva & Thybo 2013). A crustal root will result in increased buoyancy and thus elevated topography, which is possibly inconsistent with the >50 km offset between the gravity low and topographic high. Lateral changes in flexural rigidity are likely to occur on a continental margin and may contribute to the offset between a topographic high and a flexural root. A deep source like the Moho is, for example, more consistent with the geoid signal.

2.3 Scenario C: uppermost mantle

The SCLM can exhibit substantial lateral density variations stemming from changes in chemical composition and thermal thickness. The NN anomaly region is located at the continental margin where the continental lithosphere is thinning and changing into oceanic lithosphere. Furthermore is the gravity anomaly located at or close to the boundary of Proterozoic to Archaean basement. Archaean SCLM, being more depleted in iron and enriched in magnesium, has a lower bulk density and can thus provide for the low gravity.

In addition, Archaean lithosphere is generally thicker and colder, which results in a negative buoyancy effect and is thus counteracting the buoyancy effect of the lower-density mineral composition. A sliver of Archaean SCLM within otherwise Proterozoic SCLM may thus contribute to the gravity low (Fig. 6). This could also be true for NE Greenland, where the deeper lithosphere underlying the Palaeoproterozoic to Caledonian basement rocks has hardly been investigated. On the other hand, a deep source is expected to result in a smooth, large-scale gravity anomaly without the characteristic steep flanks observed in northern Norway.

2.4 Scenario D: dynamic mantle

Large-scale gravity and topographic anomalies are often explained by dynamic processes of mantle up- or downwelling (Fig. 6). Local mantle convection can occur at sharp, step-like changes in LAB depth, as they are often found on continental margins.

However, the NN anomaly is very localized but mantle convection along a thinning margin (corner flow) would likely expand much further margin parallel. Additionally, the nearly conjugate anomaly in NE Greenland would require a mechanism that leads to simultaneous mantle convection on both sides. Such a mechanism is not known of and the conjugacy as well as the isolated extent of the anomaly suggests a structural source.

3 INTEGRATED GEOPHYSICAL-PETROLOGICAL MODELLING

3.1 Method: LitMod3D

We model the lithospheric structure using the integrated geophysical modelling software LitMod3D (Afonso *et al.* 2008; Fullea *et al.* 2009). LitMod3D integrates geophysical and petrological forward modelling of the lithosphere and the sub-lithospheric mantle shallower than the transition zone within a self-consistent thermodynamic framework. By solving the appropriate heat transfer, thermodynamical, rheological, geopotential and isostasy equations, key physical properties in the mantle (e.g. seismic velocities, density, electrical conductivity) are constrained as a function of pressure, temperature and bulk composition. The 3-D density and temperature distributions within the model domain are iteratively estimated before computing geophysical observables such as the geoid, surface heat flow, gravity anomalies and isostatically adjusted topography. The approach generates thermodynamically self-consistent 3-D subsurface models that can simultaneously account for a large number of geophysical and petrological observables, thus significantly reducing the uncertainties associated with modelling these data sets separately or in pairs. The methodology and finite-element code for the 2-D version (LitMod) are described in detail in Afonso *et al.* (2008), and the extension of this methodology to 3-D modelling is described in Fullea *et al.* (2009). The modelling work flow is presented in Fig. 7.

The models comprise crust, lithospheric mantle and sub-lithospheric mantle down to a depth of 400 km. The base of the lithosphere is generally marked by a change in various physical parameters and processes, for example, strain rate, heat transfer mechanism, seismic velocity, electrical conductivity or seismic anisotropy (Eaton *et al.* 2009; Fischer *et al.* 2010; Yuan & Romanowicz 2010, and references therein). In this work, we adopt a thermal definition of the lithosphere (the 1315 C isotherm). In the lithosphere, the temperature distribution is calculated by solving the 3-D steady-state heat conduction equation using a P-T-dependent thermal conductivity (Afonso *et al.* 2008; Fullea *et al.* 2009) and considering a set of appropriate boundary conditions. In the sub-lithospheric mantle the heat transport is dominated by convection and therefore, the geotherm is assumed to follow an adiabatic gradient here (e.g. Afonso *et al.* 2008). A super-adiabatic zone in which both convection and conduction take place connects the two domains (i.e. the base of the thermal lithosphere and the adiabatic mantle).

In addition to a different thermal character, the sub-lithospheric mantle is also of more fertile composition than the colder, more rigid lithosphere. Within the lithospheric mantle, the composition is allowed to vary.

Each crustal layer in LitMod3D is characterized by its constant thermal properties and a temperature- and pressure-dependent density. The lithospheric and sub-lithospheric mantle materials are primarily characterized by their distinct major-element bulk compositions in the CFMAS scheme ($CaO–FeO–MgO–Al_2O_3–SiO_2$). Additional empirical parameters that control the pressure and temperature dependency of the thermal conductivity are taken from laboratory studies (Hofmeister 1999).

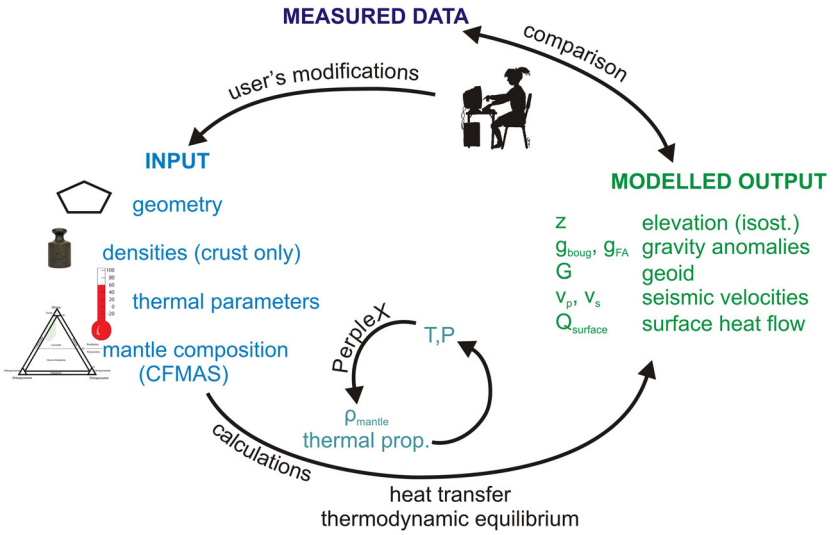

Figure 7. Simplified flow chart of LitMod3D.

Stable mineral phases in the mantle are calculated at iteratively updated pressure-temperature conditions using a scheme based on the minimization of Gibbs free energy within the major oxide system CFMAS (Connolly 2005). The bulk rock properties are averaged from the stable mineral phases based on the percentaged oxide composition. Seismic velocities in the mantle are determined according to the elastic moduli of each end-member mineral and the density of the bulk rock, as described by Connolly & Kerrick (2002).

Geoid and gravity anomalies are calculated by adding the individual contributions of a number of rectangular, flat-topped prisms of either constant or linearly varying density (Nagy *et al.* 2000; Fullea 2008). Gravity anomalies are shifted by a constant value in order to obtain a best match with the observed data and minimize the residuals. The geoid is corrected with a constant tilt, eliminating long-wavelength signals. The reader is referred to Fullea *et al.* (2009) for more technical details about the computation of the geophysical observables. The isostatic adjustment of the elevation is determined after the thermophysical calculations and is independent from other observables. It is based on the pressure distribution at the base of the model and is calculated with respect to a reference lithospheric column (Afonso *et al.* 2008). Flexural isostasy is obtained by calling an external finite-difference program (TISC, Garcia-Castellanos 2002), which requires the 2-D load distribution and a representative effective elastic thickness for the lithosphere. The flexural load is given by pressure variations at the compensation level.

The assumption that the temperature field is thermally equilibrated is not necessarily valid in the study area. The continental margin here has been subject to a major thermal event during the rifting phase *ca.* 50 Ma ago. The Iceland plume, whose main activity started around 20 Ma ago, may additionally have influenced the area although its influence has not been documented as far north as the area of interest. The thermal relaxation time for lithospheric thermal events ranges from *ca.* 50–100 Ma. The Norwegian margin is at the lower end of this spectrum, yet thermal equilibration can happen more quickly on a continental margin with thinner crust and lithosphere than in an intracontinental setting. Steady-state heat flow remains an assumption but errors associated with it (too low temperatures at the margin) are expected to yield a small, long-wavelength signal and do not directly affect our modelling results for the gravity anomaly.

3.2 Input Data

3.2.1 Geometry

A number of data sets are used to define the 3-D subsurface starting model geometrically (Table 1). These are taken from regional compilations (topography, top basement and Moho depth) and characteristics of southwestern Fennoscandia are expanded northwards (Gradmann *et al.* 2013). This starting model is then subsequently modified to test different scenarios as described and discussed in Section 4.

The topography is taken from the Scripps/NOAA global data set (Smith & Sandwell 1997). The offshore sedimentary thickness is derived from the top basement map of Norway and its continental shelf (Ebbing & Olesen 2010) and extended with the NOAA global sediment thickness data set (Divins 2012).

Various Moho depth maps covering northern Europe have been published in the past decades (Kinck *et al.* 1993; Grad *et al.* 2009; Artemieva & Thybo 2013). We use a compilation by Ebbing *et al.* (2012) of the most recent refraction seismic data sets from southern Norway (Svenningsen *et al.* 2007; Stratford *et al.* 2009) and the Moho map by Grad *et al.* (2009). Uncertainties are approximately 3–4 km in our study area (Grad *et al.* 2009). The newer compilation of Artemieva & Thybo (2013) does not include additional data onshore Fennoscandia and thus does not improve the Moho uncertainty in our study area.

The internal crustal structure in northwestern Fennoscandia has been mapped by the Blue Road deep seismic profile (Lund 1979) and shows a very uniform layering with two crustal interfaces. Similar results are obtained by more recent seismic surveys from southern Norway (Stratford *et al.* 2009). For simplicity, the layering of Stratford *et al.* (2009) has been adopted and expanded further to the east and north across the model domain, consistent with regional 2D gravity models in the study area (Ebbing *et al.* 2012). A thinning of the middle crust has been introduced towards the offshore regions. The TIB extent is chosen according to (large-scale interpolated) geological mapping with a depth range of 10–15 km. The LCL is seismically imaged in parts of Norway, Sweden and Finland (Henkel *et al.* 1990; Luosto 1997; England & Ebbing 2012). It seems to be absent in the northernmost, Archaean parts of western Fennoscandia. Its depth and thickness distribution are here taken from the isostatic models of Ebbing (2007). A more detailed crustal structure (Caledonian nappes, lateral density variations), which is in large parts determining the shorter wavelength geophysical signals, has been omitted to reduce complexity.

The lithosphere-asthenosphere boundary (LAB) marks a region at the base of the lithosphere where a number of physical parameters change (rheology, heat transfer mechanism, seismic velocity, electrical conductivity, seismic anisotropy etc.). The depth of this boundary (or layer) therefore depends on which physical parameters are mapped and which geophysical methods are used. Compilations of LAB depths under western Fennoscandia comprise teleseismic measurements (Calcagnile 1982; Plomerová *et al.* 2008), thermal

Table 1. Data sets used to constrain the starting model.

Data set	Region	Reference
Model geometry		
Elevation/bathymetry	Global	Scripps/NOAA data set, Smith & Sandwell (1997)
Basement/sediment thickness	Norwegian margin/global	Ebbing & Olesen (2010), NOAA data set, Divins (2012)
Moho depth	Fennoscandia	Compilation, Grad *et al.* (2009); Kinck *et al.* (1993); Stratford *et al.* (2009)
Thickness of lower crustal layer	Western Fennoscandia	Ebbing (2007)
Base lithosphere	Fennoscandia	Calcagnile (1982), Gradmann *et al.* (2013)
Geophysical observables		
Elevation/bathymetry	global	Scripps/NOAA data set, Smith & Sandwell (1997)
Bouguer gravity	global	DTU2010, Andersen *et al.* (2010)
Free-air gravity	global	DTU2010, Andersen *et al.* (2010)
Geoid	global	EGM08, Pavlis *et al.* (2008)

Table 2. Thermophysical properties of crustal material.

Layer	Density ρ/ (kg m^{-3})	Thermal conductivity k/ (W m^{-1} K^{-1})	Heat Production rate A/ (μW m^{-3})
Shallow sediment	2300	2.5	2.0
Deep sediment	2550	2.5	2.0
TIB	2680 (2650)	2.4	1.6–2.3
Upper crust	2750	2.4	1.6–2.3
Middle crust	2850	2.4	0.5
Lower crust	2950	2.0	0.4
Lower crustal layer (LCL)	3180	2.0	0.4
Upper oceanic crust	2850	3.3	0.01
Lower oceanic crust	3000	3.3	0.01

modelling (Balling 1995; Artemieva *et al.* 2006) and local magnetotelluric measurements (e.g. Henkel *et al.* 1990; Korja *et al.* 2008; Jones *et al.* 2010). Whereas all these data sets show a gradual depth increase from west to east in the study area, the situation is different in southern Norway and Sweden. Here, a relatively abrupt change in lithosphere thickness as well as composition has been suggested by multiple studies (Plomerová *et al.* 2008; Medhus *et al.* 2009; Gradmann *et al.* 2013). This lithospheric step is necessary to satisfy the data sets of tomography, gravity and elevation. In this study, we extrapolate these findings to the north and model a thicker lithosphere (200 km) under the Palaeoproterozoic Svecofennian domain and thinner lithosphere (100–150 km) under the younger domains of southern Norway, the coastal and the offshore areas. These are first-order assumptions but yield an overall acceptable fit to the surface observables and are consistent with the present-day understanding of the tectonic evolution of Fennoscandia.

3.2.2 *Crustal thermophysical properties*

The crustal densities (Table 2) are chosen according to previous gravity studies and surface rock measurements (Olesen *et al.* 2010; Ebbing *et al.* 2012; Gradmann *et al.* 2013). The origin of the high-density, high-velocity lowermost crust is debated and explanations range from eclogized overthickened crust to subducted oceanic crust and mafic underplating (Korsman *et al.* 1999; Cook *et al.* 2010). Our high LCL model density (3180 kg m^{-3}) is consistent with an eclogitic nature of the lower crustal layer but is not contradicting other origins. We here take the view that the modelled LCL mainly reflects the strong density increase with depth in thick continental crust, but do not propose a particular origin. The density of the TIB granites is set to 2680 kg m^{-3} (2650 kg m^{-3} in model A). Mantle densities are derived based on the major-element compositions, temperature and pressure as described in Section 3.1.

Heat production in the crust decreases with depth, values of 1–2.7 μW m^{-3} have been derived from thermal modelling for the upper crust (Kolstrup *et al.* 2012), 0.6–3 μW m^{-3} from geochemical analysis of surface rocks (Olesen *et al.* 2007; Slagstad 2008). The values chosen for this study fall into this range of data (2.0 and 1.8 μW m^{-3} for sediments and upper crust, 0.4 and 0.5 μW m^{-3} for middle and lower crust, respectively). The granites of the TIB are modelled with a variable heat production rate of 1.6–2.3 μW m^{-3}. Values of up to 3.0 μW m^{-3} are reported from petrophysical measurements of subsurface samples of the TIB in Fennoscandia (Slagstad *et al.* 2009), whereas measurements from granites around the study area show much lower values of 1.5–2 μW m^{-3} (Olesen *et al.* 2007). Thermal conductivities are described by a value of 2.5 W m^{-1} K^{-1} for sediments, 2.4 W m^{-1} K^{-1} for the upper and middle crust and 2.0 W m^{-1} K^{-1} for the lower crust (Slagstad *et al.* 2009; Kolstrup *et al.* 2012).

3.2.3 *Mantle composition and thermophysical properties*

Mantle composition generally varies with the grade of depletion and therefore with the age of the lithospheric mantle. As a rule of thumb, Archaean lithospheric mantle has the highest magnesium and lowest iron content with an average magnesium number of 92.7 (Mg# $= 100 \cdot$ Mg/(Mg + Fe), values in molar percent) and lowest bulk densities; Phanerozoic lithospheric mantle has lower magnesium and higher iron content (Mg# approx. 89.9) and higher bulk densities (e.g. Djomani *et al.* 2001; Griffin *et al.* 2009). The division into two lithospheres of distinctly different composition for southern Norway and southern Sweden (thinner, Phanerozoic-type SCLM vs. thicker, Proterozoic-type SCLM, Gradmann *et al.* 2013) is expanded to the north tracing the edge of the Baltic shield (Fig. 8a).

We use average compositions based on the tectonothermal age of the mantle terranes (Phanerozoic, Proterozoic, sub-lithospheric) as compiled by Afonso *et al.* (2008) (Table 3). These are almost certainly not representing the true SCLM compositions in the study area, but can nevertheless approximate physical properties and especially their vertical and lateral variations to first order.

The mantle compositions are defined in terms of the weight percentages of the five most abundant oxides (CFMAS system). These oxides are the main constituents of the most common upper mantle minerals (olivine, orthopyroxene, clinopyroxene, spinel, garnet, pyroxene, ringwoodite, wadsleyite) (Stixrude & Lithgow-Bertelloni 2005). Other elements constitute only minor parts (*ca.* 1 per cent) of the bulk mantle composition, yet their influence can be significant in some physical properties like seismic velocities and electrical conductivities.

The thermophysical properties of the stable mineral assemblages are calculated using the set of parameters given in Table 3. These empirical parameters refer to the bulk rock for a generic SCLM rather than to the individual minerals because the uncertainty of the controlling parameters yields variations in thermal conductivity that are of the same order as the compositional dependence. The values for the two different SCLM bulk compositions used in this study (Phanerozoic-type and Proterozoic-type) are the same as used by Gradmann *et al.* (2013).

3.2.4 *Geophysical observables*

A number of geophysical data sets are used to constrain the model by comparison with the modelled observables (Table 1). The

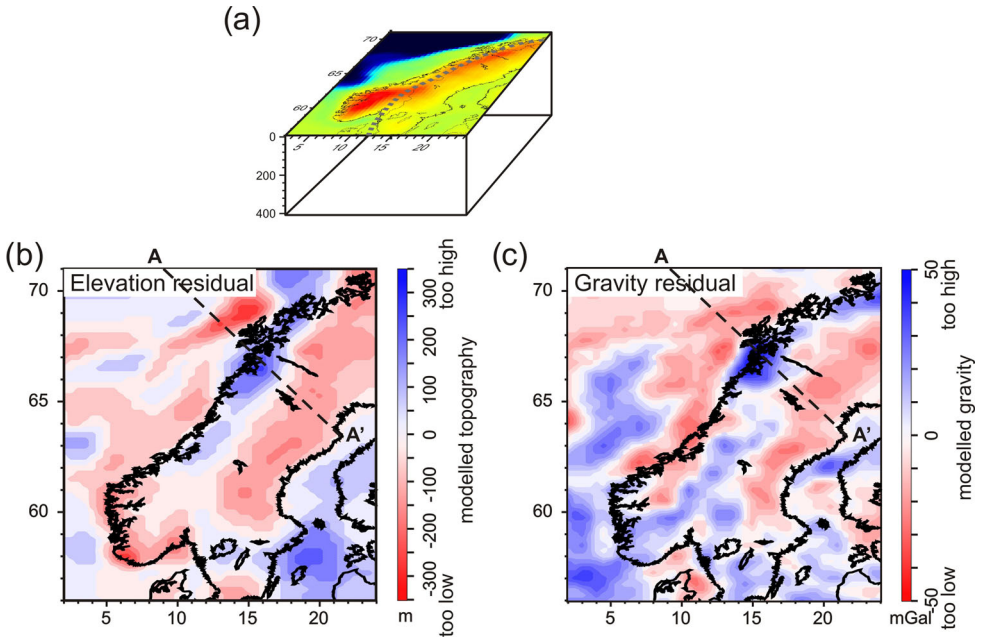

Figure 8. Starting model M0. (a) Model domain. Dashed grey line shows the approximate location of the lateral transition zone between Phanerozoic-type and Proterozoic-type SCLM. (b) Resulting elevation residual (calculated − measured). (c) Bouguer gravity residual (calculated − measured). Line *A*–*A*′ indicates the profile shown in Figs 9, 10, 12 and 13.

Table 3. Thermophysical properties of mantle materials. Mantle compositions taken from Afonso *et al.* (2008).

	Symbol	Unit	Phanerozoic mantle	Proterozoic mantle	Sublithospheric mantle
Thermal parameters					
Heat production rate	A	μW m^{-3}	0.01	0.001	0.0
Thermal expansion coefficient	α		0.31×10^{-4}	0.31×10^{-4}	0.3×10^{-4}
Reference thermal conductivity	k_0	W m^{-1} K^{-1}	5.3	4.5	0.0
Grüneisen parameter	γ		125	125	–
Isothermal bulk modulus	K_T	GPa	4.3	4.3	–
K_T pressure derivative dK_T/dP	K_0		130	130	–
Composition					
SiO_2		per cent	44.5	44.6	45.0
Al_2O_3		per cent	3.5	1.9	4.5
FeO		per cent	8.0	7.9	8.1
MgO		per cent	39.8	42.6	37.8
CaO		per cent	3.1	1.7	3.6
Mg#			89.9	90.6	89.3

geoid is taken from EGM2008 (Pavlis *et al.* 2008) with removal of the low-wavelengths of spherical harmonic order and degree lesser than ten. Bouguer and free-air anomalies are taken from the DTU2010 data set (Andersen *et al.* 2010). Bouguer reduction densities are 2670 and 1670 kg m^{-3} for onshore and offshore areas, respectively.

A regional heat flow data set of Norway has been compiled by Slagstad *et al.* (2009). These data are strongly influenced by local anomalies, insufficiently understood palaeoclimatic effects and perhaps ground water flow (Maystrenko *et al.* 2015) and can therefore only provide a rough guideline to the regional modelling.

Similarly, seismic mantle velocities are only considered qualitatively in this study. Regional tomographic data sets exist, but data coverage is sparse and its regional resolution very coarse (Legendre *et al.* 2012; Rickers *et al.* 2013).

4 RESULTS OF REFERENCE MODEL AND ITS VARIATIONS

4.1 Reference model M0

The initial 3-D subsurface model is based on the newest available data and geological understanding of the study area but is not optimized to match the observed data. Because the highest elevation occurs nearly 100 km inland of the free-air gravity low, the link between gravity and topography is highly complex. This is clearly revealed in the comparison of the model's calculated elevation and gravity signals to the observed data (Figs 8b and c). The modelled topography is too high (by up to 250 m, indicating too strong buoyancy, meaning a mass deficit), the modelled gravity is also too high by up to 40 mGal (indicating excess mass). A NW–SE cross section through the largest residual (Fig. 9, location shown in Fig. 8)

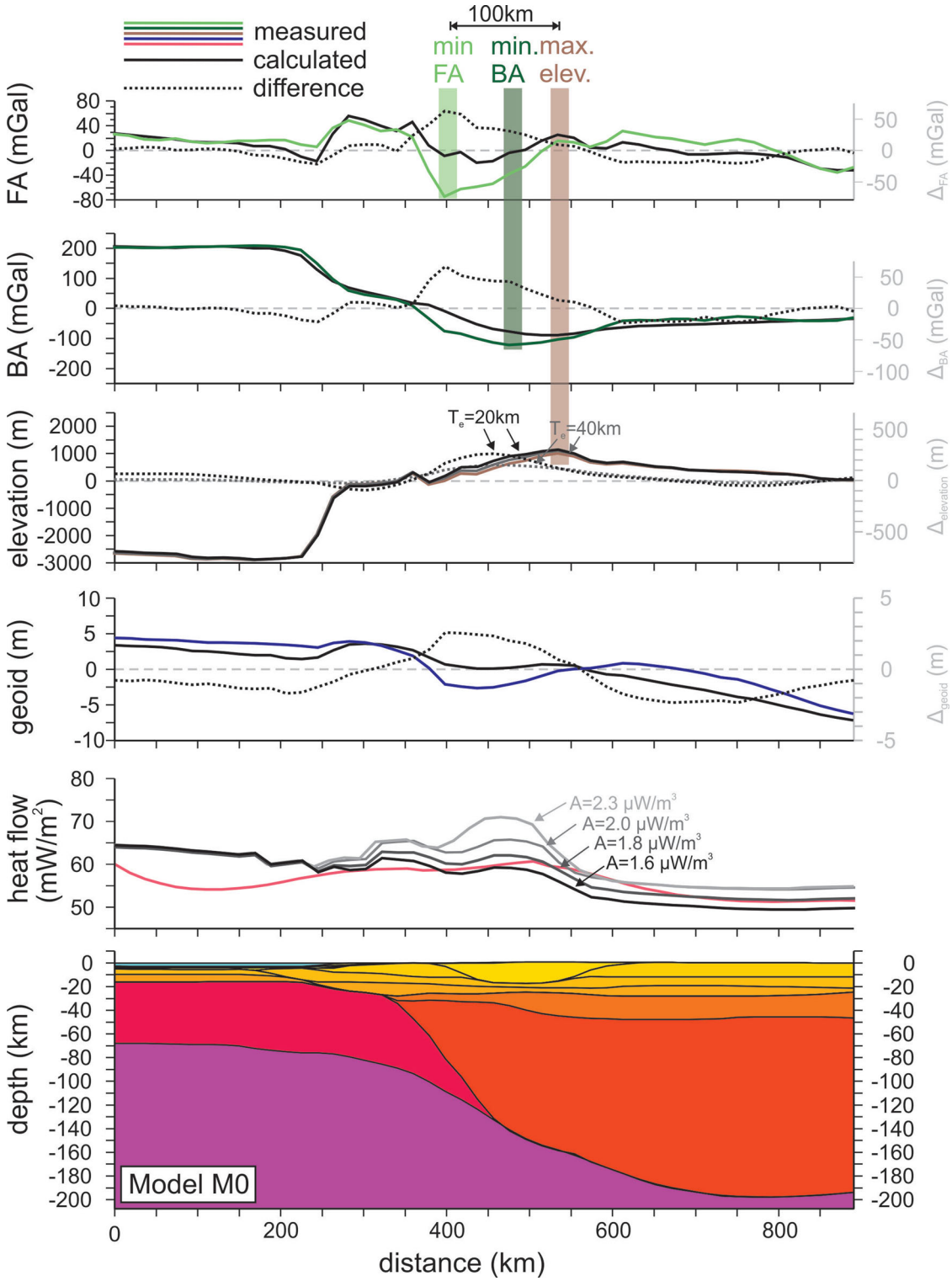

Figure 9. NW–SE cross section of model M0, location is shown in Fig. 8. Geometry is displayed in bottom panel with colours indicating different layers with different physical properties. See Tables 2 and 3 for more details. Top five panels show the measured (coloured lines) and calculated (black lines) values of free-air anomaly, Bouguer anomaly, topography, geoid and surface heat flow. The respective residuals are displayed as grey dashed lines. Calculated topography is shown for two different effective elastic thicknesses. Calculated heat flow is shown for three different heat production values of upper crust and TIB.

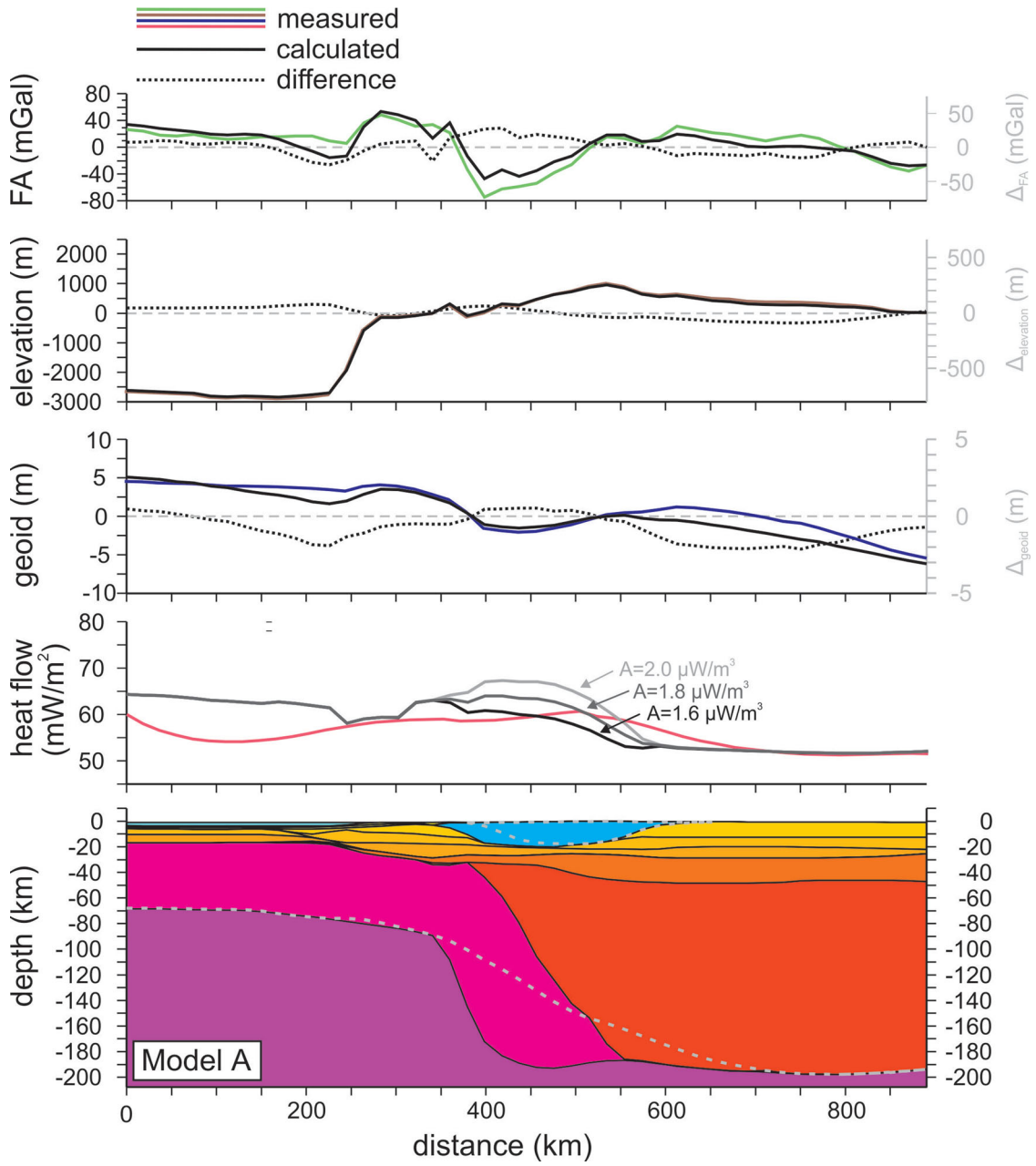

Figure 10. NW–SE cross section of model A with modifications to TIB and LAB depth. Location is shown in Fig. 8. Geometry is displayed in bottom panel with colours indicating different layers with different physical properties. See Tables 2 and 3 for more details. Dashed grey lines show the geometry of model M0. Top four panels show the measured (coloured lines) and calculated (black lines) values of free-air anomaly, topography, geoid and surface heat flow. The respective residuals are displayed as grey dashed lines. Calculated heat flow is shown for three different heat production values for the TIB.

additionally shows that the elevation and gravity anomalies are offset to each other. The highest elevation occurs at a distance of 550 km along the profile. Respective low values of −100 mGal are seen in the Bouguer gravity here, but reach even lower values at a distance of 480 km, which must be caused by other sources than the Bouguer reduction of the topography. The part of the gravity-low that is uncorrelated to the topography is clearly seen in the free-air anomaly, where the minimum value of −80 mGal lies at a distance of *ca.* 400 km. This data set is subsequently used for the comparison of modelled and measured gravity. The largest geoid anomaly of −2 m is also located around a distance of 400 km. As a consequence of this offset in the anomalies, the residuals (difference between model and observed values, dashed grey line) also occur slightly offset to each other. Elevation residuals above a flexing plate are shown for effective elastic thicknesses of $T_e = 20$ km and $T_e = 40$ km, which represent moderate to very high values for continental margins and only compensate the relatively long-wavelength structures. The fit of the geoid is relatively poor; the subhorizontal layering used here cannot adequately represent the geoid signal at the ends of the profile. Nevertheless, the following model experiments show that the geoid can locally be modified and fitted in the centre of the profile.

The calculated surface heat flow is only poorly matching the measured one, the latter being only an interpolation from measurements located relatively far away. No attempts were made to match the heat flow in the oceanic domain. Variations of the heat production rate of upper crust and TIB suggest that a value of 1.8 µW m^{-3} provides

an appropriate starting model, which is used for the subsequent models. Heat production rates for the TIB are varied and discussed for the following models. It is not possible to further constrain the thermal properties until better heat flow data become available.

All residuals occur in the region where significant lithospheric changes take place: thickness and composition of the SCLM vary, and both the LCL and the TIB taper out westwards.

The following three models show how different low-density sources could explain the gravity low. Changes in density not only affect the gravity signal but also the isostatic balance. In order to decouple these two effects to a certain degree, we additionally invoke density changes at large depth, that is, changes in lithosphere thickness. These mass changes are seated at great depth, barely affect the gravity signal, but significantly reduce the lithosphere's buoyancy. We do not model scenario D, which assumes a dynamic source (Fig. 6), because we do not consider mantle convection an appropriate mechanism for gravity anomalies that are of sub-regional small extent (100 × 150 km) and that occur on the conjugate sides of a passive margin.

4.2 Model A—TIB

4.2.1 Results

In model A, the shape and density of the TIB are adjusted in order to match the gravity signal (Fig. 12). The density difference between TIB and surrounding crust is now 100 kg m^{-3}. As a consequence of the net mass removal, buoyancy increases. In order to simultaneously match the elevation data, the LAB is lowered. The overall result shows a reasonably good fit with the gravity and topography. Remaining residuals are <20 mGal and <200 m, respectively. The remaining geoid residual is less than 1 m.

The TIB location is expanded westward with respect to the starting model and is now extending beyond the coastline, stretching nearly as much offshore as onshore. Its largest thickness is 22 km. If a higher TIB density was chosen (e.g. 2670 kg m^{-3} instead of 2650 kg m^{-3}), the thickness would need to be increased by 2–3 km. TIB densities in previous studies range from 2640–2690 kg m^{-3} (Skilbrei *et al.* 2002; Pascal *et al.* 2007; Ebbing 2007). With the low TIB-density of model A, the crustal thickness below the TIB is *ca.* 10 km, which is low, but still a significant part of the entire crust. The discrepancy between calculated and measured heat flow is now larger than in model M0.

The deep cratonic LAB is extended to the margin such that it underlies the gravity low. A Phanerozoic-type composition is assumed for this additional 'root'. A Proterozoic-type composition (lower bulk densities) would result in larger buoyancy and remaining elevation residuals of nearly 500 m. It seems plausible to assume that the thick SCLM under the gravity anomaly was originally of a more depleted composition but later metasomatized during the rifting process, leading to refertilization and higher bulk densities.

4.2.2 Discussion

The actual extent of the TIB in northern Norway is poorly known and concealed by the Caledonian nappes (Fig. 2), although some tectonic windows exist in northern Norway and some parts of the Lofoten-Vesterålen archipelago. To the south and east, it is outcropping in Sweden and has been geophysically mapped under the Caledonian nappes in central Norway and Sweden (Skilbrei *et al.* 2002; Olesen *et al.* 2010). Where it forms the visible bedrock, the respective gravity anomaly is significantly less pronounced than in northern Norway. TIB samples from northern Norway show densities of 2660–2670 kg m^{-3}, which has been confirmed by gravity modelling (Olesen *et al.* 1997). The large magnetic anomaly in northern Norway (Fig. 4a) is located to the southeast of the gravity anomaly. Directly at the location of the anomaly, only moderately high magnetic intensity is recorded. In general, both the surface geology and magnetic data suggest that the TIB extends to the east of the gravity anomaly and thus lies much more east than the TIB of model A.

The 20 km thick TIB in model A yields surface heat flow values of close to 70 mW m^{-2} with heat production rate and thermal conductivity of 2.0 μW m^{-3} and 2.4 W m^{-1} K^{-1}, respectively. Such heat flow values are somewhat higher than elsewhere in Fennoscandia, although equally high values have been found above the TIB in central Sweden (Slagstad *et al.* 2009). In the region of the NN anomaly, values of only 50 mW m^{-2} have been reported (Olesen *et al.* 2007). Heat production rates measured in the Fennoscandian granites vary significantly, reaching very high values locally (up to 3 μW m^{-3}, Pascal *et al.* 2007; Slagstad *et al.* 2009) but also showing very low values, especially close to the study area (less than 1.5 μW m^{-3}, Olesen *et al.* 2007). A heat production rate of much larger than 2.0 μW m^{-3}, as measured in TIB granites elsewhere in Fennoscandia (Slagstad *et al.* 2009), seems too high, but more data needs to be awaited before better constraints of the thermal properties are possible.

In a thermo-rheological study from central Norway and Sweden, Pascal *et al.* (2007) showed that a 20 km thick TIB leads to very high heat flow values, a Moho temperature around 750 °C (close to melting temperatures) and an unreasonably low lithospheric strength. They thus conclude that a TIB thickness of around 12 km is in closer agreement with the data.

The conjugate margin of Greenland exhibits a strikingly similar gravity anomaly, covering both onshore and offshore areas. The anomaly is 500 × 200 km large and *ca.* 100 mGal in magnitude. Two major basins exist offshore, but only the more proximal, older and deeper Danmarkshavn Basin falls into the extent of the gravity low (Fig. 11). This gravity low has been mentioned in Hamann *et al.* (2005), but no model or interpretation has been brought forward yet. Palaeo-reconstructions align the NE Greenland gravity anomaly with the NN anomaly as if it was a direct northward extension (Fig. 1).

When the TIB was emplaced during the late Palaeo- to Mesoproterozoic (pre-Rodinia), it was likely southern Greenland that was aligned with Baltica (Fig. 11b). Here, evidence for subduction-related arc magmatism not unlike the Scandinavian TIB is seen (Zhao *et al.* 2002). NE Greenland itself does not expose any TIB-like granites but consists primarily of older, Palaeoproterozoic gneisses that were formed 2.5–2.3 Ga ago (Fig. 11 a Kalsbeek *et al.* 1993). These gneisses form the Caledonian foreland, at present largely covered by the Greenland ice sheet as well as the nappes that were thrusted westward during the Caledonian orogeny (Fig. 11a). The easternmost thrust sheets also contain Meso- and Neoproterozoic mafic intrusions and metasediments. Ultra-high pressure rocks of late or even past-Caledonian ages are found in the North East Greenland Eclogite Province on Germania Land (Gilotti & Ravna 2002; Gilotti *et al.* 2008). An isolated occurrence of Archaean rocks has been reported from southern Germania Land (Steiger *et al.* 1976; Kalsbeek *et al.* 2008). The geological field evidence thus indicates high-density rocks but no granite-like near-surface structure. The fairly round shape of the Greenland anomaly is likewise inconsistent with a belt-like formation like the TIB.

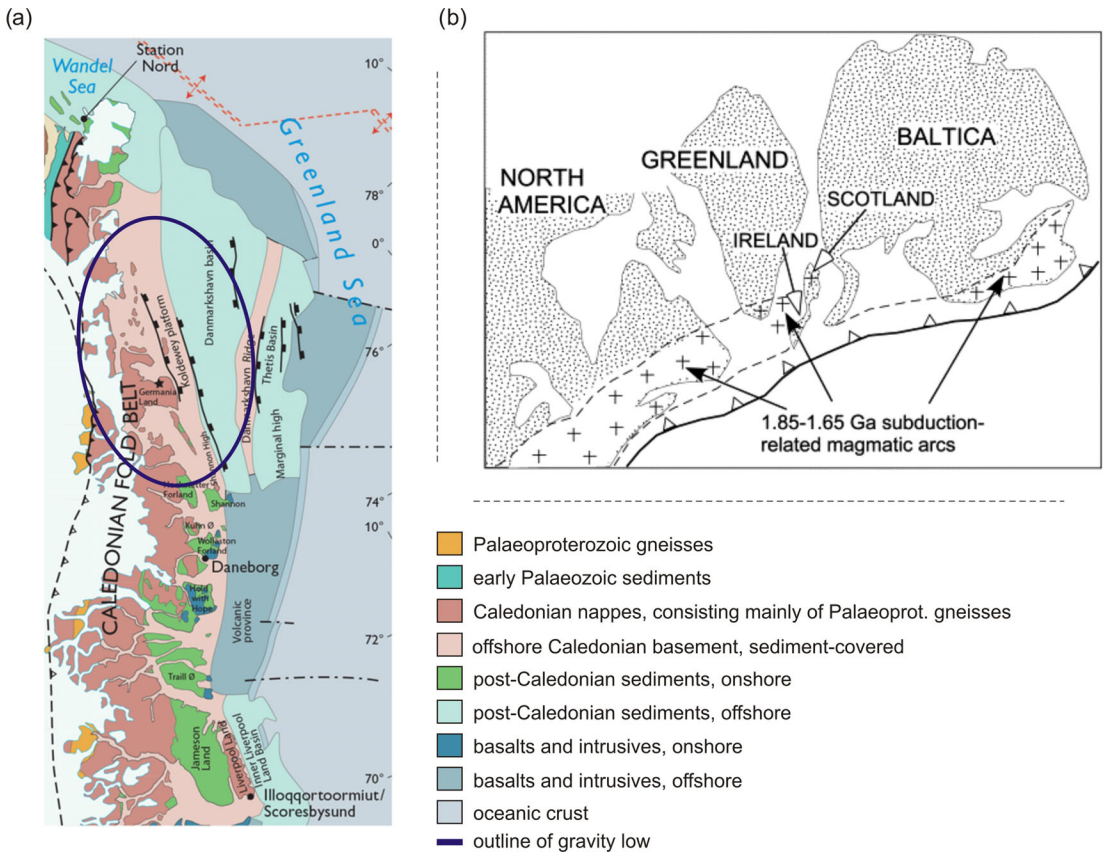

Figure 11. (a) Geology of NE Greenland. After Hamann *et al.* (2005) and Henriksen (2008). (b) Late Palaeoproterozoic reconstruction showing positions of old cratons and subduction-related arc-magmatism. From Zhao *et al.* (2002) and Park (1992).

Despite the good fit of model A, we do not consider it likely that the TIB is the only source of the NN gravity low. Neither its overall extent in Fennoscandia nor its absence in NE Greenland is consistent with this interpretation.

4.3 Model B—lower crustal structure

4.3.1 Results

This model combines changes to the LCL and the Moho. The LCL of the starting model (see Ebbing 2007) does not extend far enough to the west to have a significant influence on the region with the gravity low. We modify the LCL where it exists and change the Moho depth otherwise (Fig. 12). The Moho is lowered to form a crustal root under the gravity low. The same SCLM geometry as in model A is chosen. The fit of the gravity is acceptable (residuals of 25 mGal), the elevation residual remains at 300 m and thus does not constitute an improvement to the starting model. The geoid and heat flow both show a relatively poor fit.

4.3.2 Discussion

The crustal structure of the Nordland region is poorly studied. Moho compilations show a thinning crust along the Lofoten margin and Moho depths of *ca.* 30–36 km under the NN anomaly (Grad *et al.* 2009; Artemieva & Thybo 2013). The closest deep seismic profile runs offshore and almost reaches the southern end of the NN anomaly, where it shows Moho depths of 25 km (Mjelde *et al.* 1993). The closest onshore seismic experiments lies *ca.* 100 km to the south of the anomaly and images Moho depths of >40 km (Lund 1979). A very recent receiver function profile which runs just north of the anomaly indicates Moho depths of *ca.* 40 km right up to the Lofoten archipelago (Mansour *et al.* 2014). Overall, these data suggest that the onshore region is indeed underlain by fairly thick crust which thins rapidly towards the offshore regions. Local variations in Moho depth and lower crustal structure would be consistent with the current, admittedly relatively poor knowledge of the crustal structure around the NN anomaly.

On the conjugate side in Greenland, Moho depths of *ca.* 28–32 km have been reported (Artemieva & Thybo 2013). Again, these values are widely interpolated or extrapolated and do not constrain the local Moho depth very well.

The crustal root has a strong buoyancy effect, which in the present model is to a first degree compensated by a very thick lithosphere. This ‘cold thermal root’, so to speak, exerts negative buoyancy owing to the higher density of the colder rocks. It nevertheless barely manages to compensate for the additional buoyancy of the crustal root. In Greenland, a local crustal root of several kilometres thickness would be inconsistent with below-sea-level topography and offshore deposition of up to 10 km thick sediments.

4.4 Model C–Archaean SCLM

4.4.1 Results

In model C, an Archaean sliver is added to the otherwise Proterozoic SCLM. Its more depleted composition and hence lower density lead to a reduced gravity signal. The shape and size are chosen to match the gravity anomaly to first order. The LAB is lowered to *ca.* 200 km

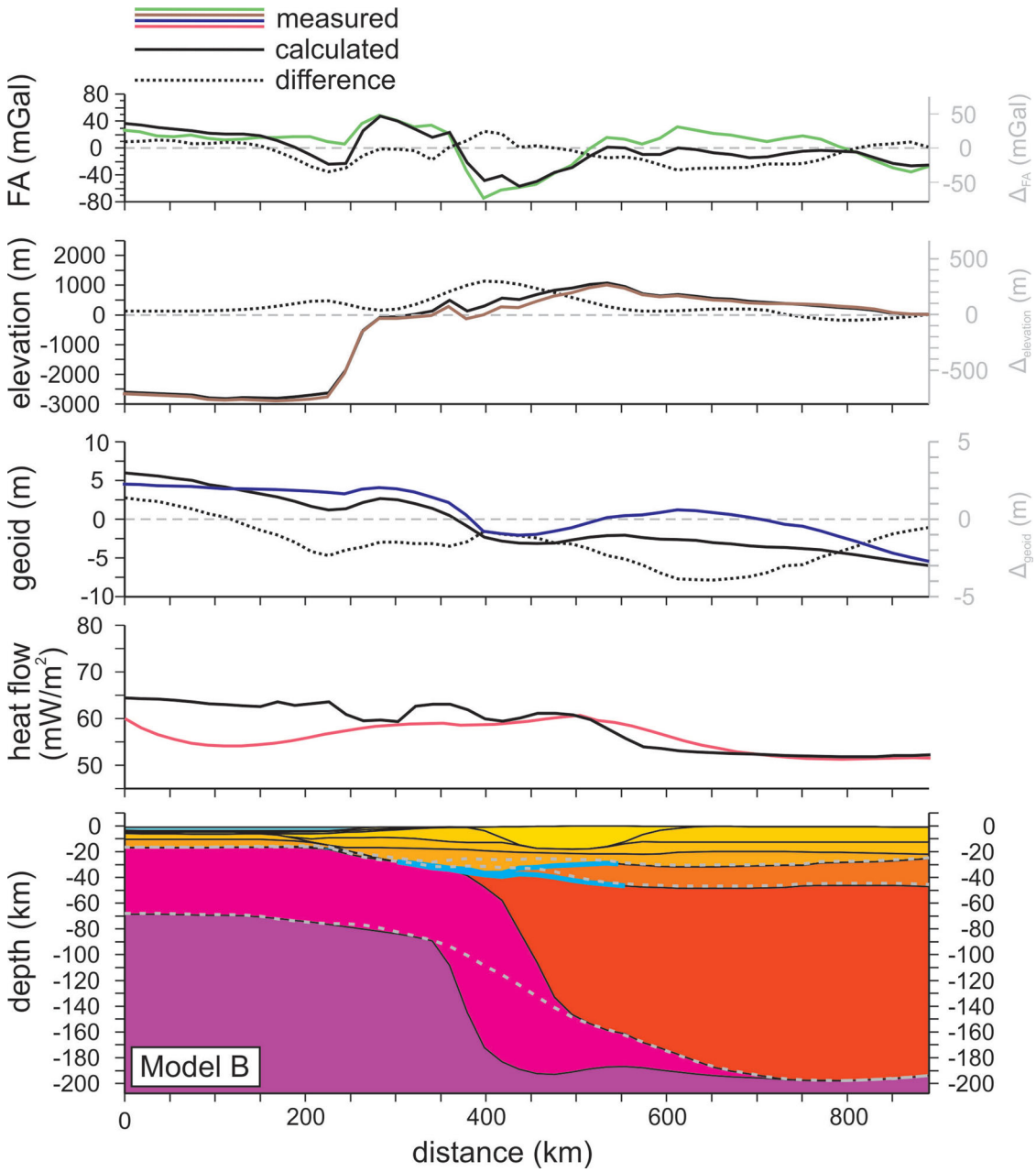

Figure 12. NW–SE cross section of model B with modifications to LCL, Moho and LAB depth. Location is shown in Fig. 8. Geometry is displayed in bottom panel with colours indicating different layers with different physical properties. See Tables 2 and 3 for more details. Dashed grey lines show the geometry of model M0. Top four panels show the measured (coloured lines) and calculated (black lines) values of free-air anomaly, topography, geoid and surface heat flow. The respective residuals are displayed as grey dashed lines.

as in previous models. Whereas the calculated and measured gravity and geoid signal show some agreement (matching shape, residual of 60 mGal and 1 m, respectively), the calculated topography is far off the actual one, residuals are up to 350 m. A lowering of the LAB to 250–300 km reduces this residual, but introduces a long-wavelength misfit. The calculated heat flow is reduced by the Archaean SCLM and the lowered LAB and now provides a reasonable fit.

4.4.2 Discussion

The transition between Archaean and Palaeoproterozoic crust in northern Norway is not well mapped. Proterozoic sediments as well as the Caledonian nappes overlie older cratonic basement. The FENNOLORA reflection seismic profile in northern Sweden and northernmost Norway succeeded to differentiate between the Proterozoic and Archaean terranes (Clowes *et al.* 1987; Henkel *et al.* 1990; Guggisberg *et al.* 1991; Luosto 1997). The latter is generally characterized by somewhat lower densities and seismic velocities in the lower crust and a lack of the LCL. Archaean rocks have been mapped locally on the Lofoten peninsula and through some basement windows under the Caledonian nappes. It is thus not unlikely that Archaean rocks are present towards the southeast under the Caledonian nappes where the NN anomaly lies, but may simply have not been exhumed.

In magnetic anomaly maps, the Archaean craton appears with a higher magnetic intensity (Fig. 4a). In our study area, however, this characteristic is difficult to differentiate from the potentially high susceptibility of the rocks of the TIB as well as from

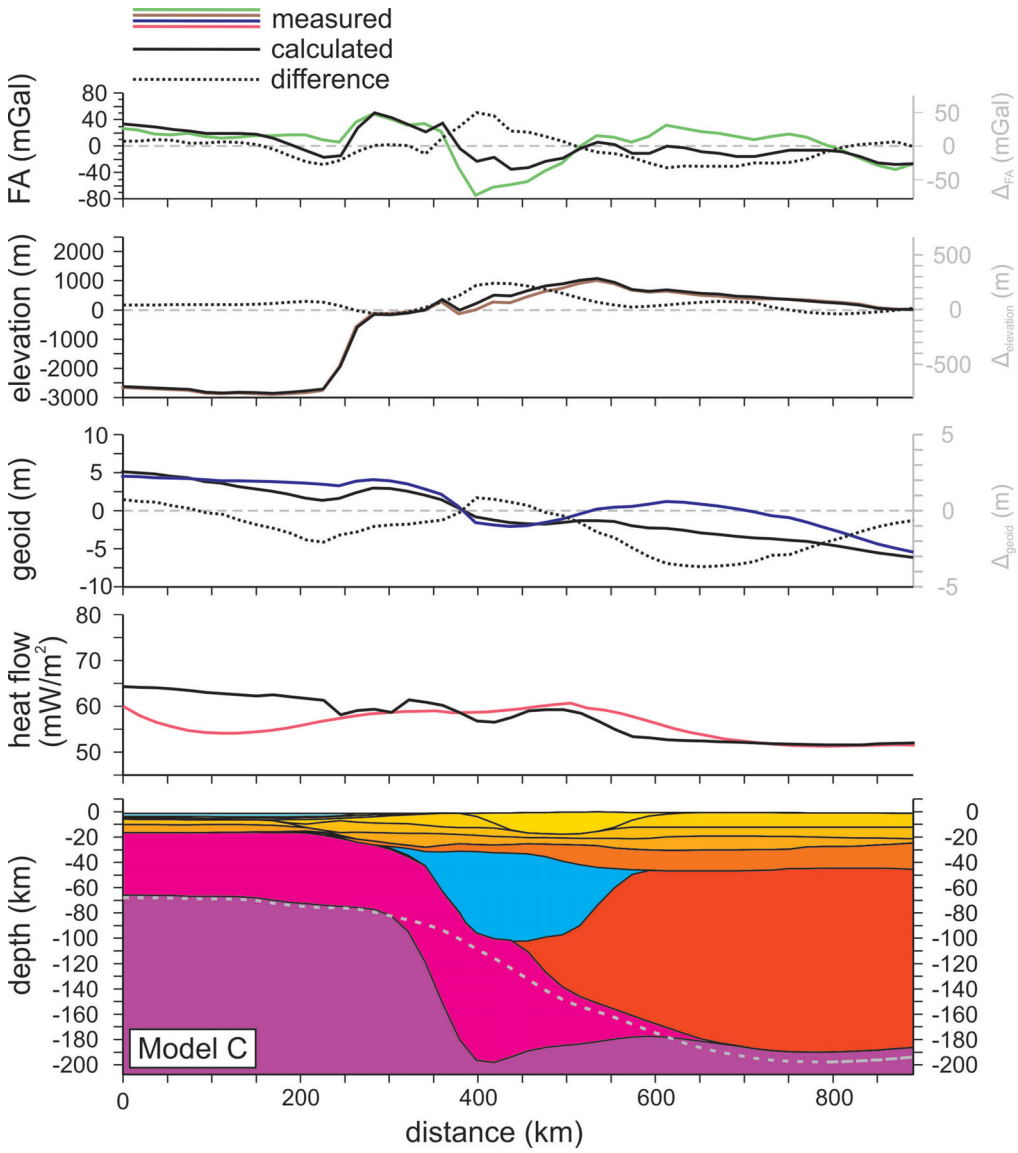

Figure 13. NW–SE cross section of model C with modifications to SCLM composition and LAB depth. Location is shown in Fig. 8. Geometry is displayed in bottom panel with colours indicating different layers with different physical properties. See Tables 2 and 3 for more details. Dashed grey lines show the geometry of model M0. Top four panels show the measured (coloured lines) and calculated (black lines) values of free-air anomaly, topography, geoid and surface heat flow. The respective residuals are displayed as grey dashed lines.

the structures at larger depth. The Proterozoic-Archaean boundary in the SCLM (at >40 km depth) may be somewhat offset to the equivalent structural geological boundary observed near the surface.

In NE Greenland, a mantle contribution to the gravity low is a tempting explanation because only the surface rocks have been studied, but the deeper lithospheric structure remains unknown. On the other hand, the issue of too high buoyancy would be even more prominent in NE Greenland, where part of the anomaly lies offshore, where buoyancy is obviously low. A sliver of Archaean SCLM has effects on seismic velocities, heat flow as well as the geoid. Its different composition leads to locally higher seismic mantle velocities. This is not seen in tomographic studies (Bannister *et al.* 1991; Legendre *et al.* 2012; Rickers *et al.* 2013), but the structures directly below the Moho are generally poorly resolved by this method. Teleseismic data from other elsewhere in Archaean Fennoscandia have locally resolved high-velocity sub-Moho structures (Bruneton *et al.* 2004).

5 DISCUSSION

The models show that none of the simple modifications (TIB, lower crustal structure or SCLM) is sufficient to explain both the gravity and topographic data of northern Norway simultaneously. The best overall fit is obtained with a strong contribution from a shallow-source structure that lies under the coastal anomaly. Nevertheless, it is perhaps not justified to equate this shallow-source structure with the TIB. In areas where the presence of the TIB is well documented by geological mapping and magnetic data, the gravity response is weak. Furthermore, the NN gravity low does not coincide with the (presently known) near-surface extent of the TIB in northern Norway. This case can also be made for the NE Greenland side.

The deeper sources of the gravity anomaly (models B and C) fail to explain the relatively low topography. All models assume flexural isostatic compensation and require a lithospheric thickness of at least 200 km with an effective elastic thickness $T_e = 40$ km. Continental margins usually have a low rigidity ($T_e < 20$ km),

estimates for coastal Fennoscandia range from 25–35 km (Pérez-Gussinyé *et al.* 2004). We chose the relatively high value in order to facilitate a joint fit of gravity and topographic data and to be consistent with the thick lithosphere we postulate. A lower T_e would allow for locally even higher elevation and thus larger misfit of modelled and observed topography above the low-density anomaly source (see Fig. 8).

The assumption of isostatic equilibrium is not justified if there is presently ongoing tectonic deformation. Besides post-glacial rebound of entire Fennoscandia, there is evidence for local neotectonic activity in northwestern Fennoscandia related to local extension and relative subsidence (Olesen *et al.* 2013). Significant Neogene uplift of the Scandinavian Mountain Chain has been postulated and described by several authors (Riis 1996; Fjeldskaar *et al.* 2000; Japsen & Chalmers 2000). Ongoing uplift would result in a slightly lower gravity signal as well as lower topography than calculated in the models. This can partly be taken into consideration by choosing a relatively high T_e, which effectively oppresses the additional buoyancy in the models. A T_e of 40 km could suppress the uplift in regions of less than 100–150 km extent. The very local extent of the NN gravity anomaly as well as its conjugate counterpart oppose the hypothesis that it originates from substantial recent uplift.

The lithosphere's thermal structure is generally imaged by tomographic studies - yet a number of different studies give a very variable picture. Regional tomographic models show a lower mantle velocity under the northern Atlantic coast of Norway (Bannister *et al.* 1991; Legendre *et al.* 2012). These velocities, which indicate a hotter and thus thinner lithosphere, are similar to those of southern Norway, where a 100–120 km thick, non-cratonic lithosphere has been inferred (Gradmann *et al.* 2013). Other regional full waveform tomographic inversions see these low-velocity anomalies only in southern, but not in northern Norway (Rickers *et al.* 2013). A tomographic study using only local seismic events images a low-velocity zone offshore, whereas the onshore region of the NN gravity low is underlain by higher mantle velocities (Latif 2012). A clear lack of reliable active and passive seismic experiments is thus evident.

The models assume highly simplified lithospheric geometries. The SCLM is represented as a vertically homogeneous body of uniform composition. Especially cratonic lithospheric mantle is known to be divided into layers of different composition and different degrees of depletion. These variations (but also lateral changes) affect the buoyancy and gravity signal, though likely at a larger extent than the NN gravity low.

The offshore sediments and the rocks of the Caledonian nappes are not adequately represented in the models in order to keep resolution and complexity low. The Caledonian nappes are maximum 6 km thick (Olesen *et al.* 2002) and fully eroded over several basement windows.

As indicated before, the lack of knowledge of the crustal structure (internal layering, TIB-presence, Moho depth) limits the testing of different scenarios. Likewise is a model of the Greenland anomaly also not feasible at present, because of the even larger gap in the knowledge of the lithospheric structure and physical properties. Geophysical surveys that aim to map the Moho, LAB and crustal structure are needed.

As to the actual origin of the gravity low, we can only hypothesize at this point. A potential origin would be a combination of the tested scenarios. The combined effects of a TIB-like shallow surface feature, a larger Moho depth and an Archaean SCLM sliver will easily produce a very pronounced gravity low. However, the buoyancy effects would also add up and create an enormous topographic residual. In a test model (not shown here), this additional buoyancy could no longer be compensated by a deeper LAB, even if extended to 350 km depth. Based on the isostatic considerations, only model A with a TIB-like source for the gravity anomaly shows plausible results. Yet this interpretation is difficult to reconcile with the extent of the surrounding TIB and the gravity anomaly in NE Greenland and an additional contribution from a deeper source is suggested.

5.1 Conclusion

A prominent gravity low exists in northern Norway and on its conjugate margin in NE Greenland. A number of model geometries have been tested to explain the anomaly with sources at shallow, intermediate and large depths. None of the models properly satisfies the data sets of gravity and topography simultaneously. Yet, a number of conclusions can be drawn:

(i) The anomaly likely has a structural origin (rather than a dynamic one) because of the regionally limited extent of 100–150 km. If the gravity anomaly of NE Greenland is indeed of a similar origin, a dynamic source is not possible.

(ii) A near-surface source is most consistent with the available data sets. An additional contribution from a deeper source is suggested.

(iii) The TIB is not likely to be the sole source of the gravity low because of the absence of a strong gravity response elsewhere in Fennoscandia. A TIB-like origin is also not possible for the anomaly in NE Greenland.

(iv) A thick lithosphere (LAB depth at >200 km) is necessary in the coastal area to satisfy an isostatically compensated topography.

ACKNOWLEDGEMENTS

This work was conducted in the framework of the TopoScandiaDeep project, which was part of the TOPO-EUROPE EUROCORES programme of the European Science Foundation. Additional support was given by the Norwegian Research Council. We like to thank Odleiv Olesen for valuable discussions and Javier Fullea for his support in using the LitMod3D software. Furthermore, we appreciate the helpful comments of Niels Balling, an anonymous reviewer and the editors of GJI, which led to significant improvements of this manuscript.

REFERENCES

Afonso, J.C., Fernàndez, M., Ranalli, G., Griffin, W.L. & Connolly, J.A.D., 2008. Integrated geophysical-petrological modeling of the lithosphere and sublithospheric upper mantle: methodology and applications, *Geochem. Geophys. Geosyst.,* **9**(5), doi:10.1029/2007GC001834.

Åhäll, K.-I. & Larson, S.Å., 2000. Growth-related 1.85–1.55 Ga magmatism in the Baltic Shield; a review addressing the tectonic characteristics of Svecofennian, TIB 1-related, and Gothian events, *GFF,* **122**(2), 193–206.

Andersen, O., 2010. The DTU10 global gravity field and mean sea surface - improvements in the Arctic Ocean, in *Second international symposium of the gravity field of the Earth,* Fairbanks, AK, USA.

Andersen, O.B., Knudsen, P. & Berry, P.A., 2010. The DNSC08GRA global marine gravity field from double retracked satellite altimetry, *J. Geod.,* **84,** 191–199.

Anderson, U., 1997. Petrogenesis of some Proterozoic granitoid suites and associated basic rocks in Sweden (geochemistry and isotope geology), *Rapporter och Meddelanden - Sveriges Geologiska Undersökning,* **91**.

Arlitt, R., Kissling, E. & Ansorge, J., 1999. Three-dimensional crustal structure beneath the TOR array and effects on teleseismic wavefronts, *Tectonophysics,* **314**(1–3), 309–319.

Artemieva, I.M. & Thybo, H., 2013. EUNAseis: a seismic model for Moho and crustal structure in Europe, Greenland, and the North Atlantic region, *Tectonophysics,* **609**(0), 97–153.

Artemieva, I.M., Thybo, H. & Kaban, M.K., 2006. Deep Europe today: geophysical synthesis of the upper mantle structure and lithospheric processes over 3.5 Ga, *Geological Society, London, Memoirs,* **32**(1), 11–41.

Balling, N., 1995. Heat flow and thermal structure of the lithosphere across the Baltic Shield and northern Tornquist Zone, *Tectonophysics,* **244**(1–3), 13–50.

Bannister, S., Ruud, B. & Husebye, E., 1991. Tomographic estimates of sub-Moho seismic velocities in Fennoscandia and structural implications, *Tectonophysics,* **189**(1–4), 37–53.

Bingen, B. *et al.*, 2005. Timing of continental building in the Sveconorwegian orogen, SW Scandinavia, *Norwegian J. Geol.,* **85,** 87–116.

Bingen, B., Nordgulen, Ø. & Viola, G., 2008. A four-phase model for the Sveconorwegian orogeny, SW Scandinavia, *Norwegian J. Geol.,* **88,** 43–72.

Bruneton, M. *et al.*, 2004. Complex lithospheric structure under the central Baltic Shield from surface wave tomography, *J. geophys. Res.,* **109**(B10), doi:10.1029/2003JB002947.

Calcagnile, G., 1982. The lithosphere-asthenosphere system in Fennoscandia, *Tectonophysics,* **90**(1–2), 19–35.

Clowes, R., Gens-Lenartowicz, E., Demartin, M. & Saxov, S., 1987. Lithospheric structure in southern Sweden - results from FENNOLORA, *Tectonophysics,* **142**(1), 1–14.

Connolly, J., 2005. Computation of phase equilibria by linear programming: A tool for geodynamic modeling and its application to subduction zone decarbonation, *Earth planet. Sci. Lett.,* **236**(1–2), 524–541.

Connolly, J. & Kerrick, D., 2002. Metamorphic controls on seismic velocity of subducted oceanic crust at 100–250 km depth, *Earth planet. Sci. Lett.,* **204**(1–2), 61–74.

Cook, F.A., White, D.J., Jones, A.G., Eaton, D.W., Hall, J. & Clowes, R.M., 2010. How the crust meets the mantle: Lithoprobe perspectives on the Mohorovicic discontinuity and crust-mantle transition, *Can. J. Earth Sci.,* **47**(4), 315–351.

Cotte, N. & Pedersen, H., TOR Working Group, 2002. Sharp contrast in lithospheric structure across the Sorgenfrei-Tornquist Zone as inferred by Rayleigh wave analysis of TOR1 project data, *Tectonophysics,* **360**(1–4), 75–88.

Divins, D., 2012. *NGDC Total Sediment Thickness of the World's Oceans and Marginal Seas,* http://www.ngdc.noaa.gov/mgg/sedthick/sedthick.html, last accessed September 2014.

Djomani, Y.H.P., O'Reilly, S.Y., Griffin, W. & Morgan, P., 2001. The density structure of subcontinental lithosphere through time, *Earth planet. Sci. Lett.,* **184**(3–4), 605–621.

Eaton, D.W., Darbyshire, F., Evans, R.L., Grütter, H., Jones, A.G. & Yuan, X., 2009. The elusive lithosphere-asthenosphere boundary (LAB) beneath cratons, *Lithos,* **109**(1–2), 1–22.

Ebbing, J., 2007. Isostatic density modelling explains the missing root of the Scandes, *Norwegian J. Geol.,* **87,** 13–20.

Ebbing, J. & Olesen, O., 2005. The Northern and Southern Scandes - structural differences revealed by an analysis of gravity anomalies, the geoid and regional isostasy, *Tectonophysics,* **411**(1–4), 73–87.

Ebbing, J. & Olesen, O., 2010. New compilation of top basement and basement thickness for the Norwegian continental shelf reveals the segmentation of the passive margin system, *Geological Society, London, Petroleum Geology Conference Series,* **7,** 885–897.

Ebbing, J., England, R., Korja, T., Lauritsen, T., Olesen, O., Stratford, W. & Weidle, C., 2012. Structure of the Scandes lithosphere from surface to depth, *Tectonophysics,* **536–537,** 1–24.

Ebbing, J., Bouman, J., Fuchs, M., Gradmann, S. & Haagmans, R., 2014. Sensitivity of GOCE gravity gradients to crustal thickness and density variations: case study for the northeast Atlantic region, in *Gravity, Geoid and Height Systems, International Association of Geodesy Symposia,* Vol. 141, pp. 291–298, ed. Marti, U., Springer International Publishing.

Eken, T., Shomali, Z.H., Roberts, R., Hieronymus, C.F. & Bodvarsson, R., 2008. S and P velocity heterogeneities within the upper mantle below the Baltic Shield, *Tectonophysics,* **462**(1–4), 109–124.

England, R.W. & Ebbing, J., 2012. Crustal structure of central Norway and Sweden from integrated modelling of teleseismic receiver functions and the gravity anomaly, *Geophys. J. Int.,* **191**(1), 1–11.

Færseth, R. & Lien, T., 2002. Cretaceous evolution in the Norwegian Sea - a period characterized by tectonic quiescence, *Mar. Pet. Geol.,* **19**(8), 1005–1027.

Fischer, K.M., Ford, H.A., Abt, D.L. & Rychert, C.A., 2010. The lithosphere-asthenosphere boundary, *Annu. Rev. Earth Planet. Sci.,* **38**(1), 551–575.

Fjeldskaar, W., Lindholm, C., Dehls, J.F. & Fjeldskaar, I., 2000. Postglacial uplift, neotectonics and seismicity in Fennoscandia, *Quat. Sci. Rev.,* **19**(14–15), 1413–1422.

Fullea, J., 2008. Development of numerical methods to determine the lithospheric structure combining geopotential, lithostatic and heat transport equations. Application to the Gibraltar arc system, *PhD thesis,* Univ. de Barcelona, Barcelona, Spain.

Fullea, J., Afonso, J.C., Connolly, J.A.D., Fernàndez, M., García Castellanos, D. & Zeyen, H., 2009. LitMod3D: An interactive 3-D software to model the thermal, compositional, density, seismological, and rheological structure of the lithosphere and sublithospheric upper mantle, *Geochem. Geophys. Geosyst.,* **10**(8), doi:10.1029/2009GC002391.

Gaal, G. & Gorbatschev, R., 1987. An outline of the Precambrian evolution of the Baltic Shield, *Precambrian Res.,* **35,** 15–52.

Garcia-Castellanos, D., 2002. Interplay between lithospheric flexure and river transport in foreland basins, *Basin Res.,* **14**(2), 89–104.

Gilotti, J.A. & Ravna, E.J.K., 2002. First evidence for ultrahigh-pressure metamorphism in the North-East Greenland Caledonides, *Geology,* **30**(6), 551–554.

Gilotti, J.A., Jones, K.A. & Elvevold, S., 2008. Caledonian metamorphic patterns in Greenland, *Geological Society of America Memoirs,* **202,** 201–225.

Gorbatchev, R., 2004. The Transscandinavian Igneous Belt - introduction and background, in *The Transscandinavian Igneous Belt (TIB) in Sweden: A review of its character and evolution, Geological Survey of Finland, Special Paper,* Vol. 37, pp. 9–15, eds Högdahl, K., Andersson, U. & Eklund, O., Geological Survey of Finland.

Gorbatschev, R. & Bogdanova, S., 1993. Frontiers in the Baltic Shield, *Precambrian Res.,* **64,** 3–21.

Grad, M., Tiira, T. & ESC Working Group, 2009. The Moho depth map of the European plate, *Geophys. J. Int.,* **176**(1), 279–292.

Gradmann, S., Ebbing, J. & Fullea, J., 2013. Integrated geophysical modelling of a lateral transition zone in the lithospheric mantle under Norway and Sweden, *Geophys. J. Int.,* **194**(3), 1358–1373.

Griffin, W.L., O'Reilly, S.Y., Afonso, J.C. & Begg, G.C., 2009. The composition and evolution of lithospheric mantle: a re-evaluation and its tectonic implications, *J. Petrol.,* **50**(7), 1185–1204.

Guggisberg, B., Kaminski, W. & Prodehl, C., 1991. Crustal structure of the Fennoscandian Shield: A traveltime interpretation of the long-range FENNOLORA seismic refraction profile, *Tectonophysics,* **195**(2–4), 105–137.

Hamann, N.E., Whittaker, R.C. & Stemmerik, L., 2005. Geological development of the northeast Greenland shelf, *Geological Society, London, Petroleum Geology Conference Series,* **6,** 887–902.

Henkel, H., Lee, M.K. & Lund, C.E., 1990. An integrated geophysical interpretation of the 2000 km FENNOLORA section of the Baltic Shield, in *The European Geotraverse: Integrative Studies,* pp. 1–47, eds Freeman, R., Giesse, P. & Mueller, St., European Science Foundation.

Henriksen, N., 2008. *Geological History of Greenland,* Geological Survey of Denmark and Greenland.

Hofmeister, A.M., 1999. Mantle values of thermal conductivity and the geotherm from phonon lifetimes, *Science,* **283**(5408), 1699–1706.

Japsen, P. & Chalmers, J.A., 2000. Neogene uplift and tectonics around the North Atlantic: Overview, *Glob. Planet. Change,* **24**(3–4), 165–173.

Jones, A.G., Plomerová, J., Korja, T., Sodoudi, F. & Spakman, W., 2010. Europe from the bottom up: a statistical examination of the central and

northern european lithosphere-asthenosphere boundary from comparing seismological and electromagnetic observations, *Lithos,* **120**(1–2), 14–29.

Kalsbeek, F., Nutman, A.P. & Taylor, P.N., 1993. Palaeoproterozoic basement province in the Caledonian fold belt of North-East Greenland, *Precambrian Res.,* **63**(1–2), 163–178.

Kalsbeek, F., Thrane, K., Higgins, A., Jepsen, H.F., Leslie, A.G., Nutman, A.P. & Frei, R., 2008. Polyorogenic history of the East Greenland Caledonides, *Geological Society of America Memoirs,* **202,** 55–72.

Kinck, J., Husebye, E. & Larsson, F., 1993. The Moho depth distribution in Fennoscandia and the regional tectonic evolution from Archean to Permian times, *Precambrian Res.,* **64**(1–4), 23–51.

Kolstrup, L. M., Pascal, C. & Maupin, V., 2012. What compensates the topography of southern Norway? Insights from thermo-isostatic modeling, *J. Geodyn.,* **61**(0), 105–119.

Korja, A., Korja, T., Luosto, U. & Heikkinen, P., 1993. Seismic and geoelectric evidence for collisional and extensional events in the Fennoscandian Shield implications for Precambrian crustal evolution, *Tectonophysics,* **219**(1–3), 129–152.

Korja, T., Smirnov, M., Pedersen, L. & Gharibi, M., 2008. Structure of the Central Scandinavian Caledonides and the underlying Precambrian basement, new constraints from magnetotellurics, *Geophys. J. Int.,* **175**(1), 55–69.

Korsman, K., Korja, T., Pajunen, M. & Virransalo, P., 1999. The GGT/SVEKA transect: structure and evolution of the continental crust in the Paleoproterozoic Svecofennian orogen in Finland, *International Geology Review,* **41**(4), 287–333.

Lahtinen, R., Korja, A. & Nironen, M., 2005. Palaeoproterozoic tectonic evolution of the Fennoscandian Shield, in *Precambrian Geology of Finland - Key to the Evolution of the Fennoscandian Shield, Developments in Precambrian Geology,* Vol. 14, pp. 481–531, eds Lehtinen, P.N.M. & Rämö, O., Elsevier.

Lahtinen, R., Korja, A., Nironen, M. & Heikkinen, P., 2009. Palaeoproterozoic accretionary processes in Fennoscandia, *Geological Society, London, Special Publications,* **318**(1), 237–256.

Latif, A., 2012. Tomographic inversion of Pn waves beneath southern Scandinavia, *Master's thesis,* University of Bergen, Norway.

Legendre, C.P., Meier, T., Lebedev, S., Friederich, W. & Viereck-Götte, L., 2012. A shear wave velocity model of the European upper mantle from automated inversion of seismic shear and surface waveforms, *Geophys. J. Int.,* **191**(1), 282–304.

Lund, C.-E., 1979. The fine structure of the lower lithosphere underneath the Blue Road profile in northern Scandinavia, *Tectonophysics,* **56**(1–2), 111–122.

Luosto, U., 1997. Structure of the Earth's crust in Fennoscandia as revealed from refraction and wide-angle reflection studies, *Geophysica,* **33**(1), 3–16.

Mansour, B., Moorkamp, M. & England, R., 2014. *Joint inversion of seismological data and magnetotelluric data for the northern Scandinavian Mountains, Abstract presented at 2014 Fall Meeting*, AGU, San Francisco, CA.

Maystrenko, Y.P., Olesen, O. & Elvebakk, H.K., 2015. Indication of deep groundwater flow through the crystalline rocks of southern Norway, *Geology,*, **43**(4), 327–330.

Medhus, A., Balling, N., Jacobsen, B., Kind, R. & England, R., 2009. Deep structural differences in southwestern Scandinavia revealed by P-wave travel time residuals, *Norwegian J. Geol.,* **89,** 203–214.

Medhus, A.B., Balling, N., Jacobsen, B.H., Weidle, C., England, R.W., Kind, R., Thybo, H. & Voss, P., 2012. Upper-mantle structure beneath the Southern Scandes Mountains and the Northern Tornquist Zone revealed by P-wave traveltime tomography, *Geophys. J. Int.,* **189**(3), 1315–1334.

Mjelde, R., Sellevoll, M.A., Shimamura, H., Iwasaki, T. & Kanazawa, T., 1993. Crustal structure beneath Lofoten, N. Norway, from vertical incidence and wide-angle seismic data, *Geophys. J. Int.,* **114**(1), 116–126.

MONA LISA Working Group, 1997a. MONA LISA – Deep seismic investigations of the lithosphere in the southeastern North Sea, *Tectonophysics,* **269**(1–2), 1–19.

MONA LISA Working Group, 1997b. Closure of the Tornquist sea: constraints from MONA LISA deep seismic reflection data, *Geology,* **25**(12), 1071–1074.

Nagy, D., Papp, G. & Benedek, J., 2000. The gravitational potential and its derivatives for the prism, *J. Geod.,* **74,** 552–560.

Olesen, O., Torsvik, T., Tveten, E., Zwaan, K., Løseth, H. & Henningsen, T., 1997. Basement structure of the continental margin in the Lofoten-Lopphavet area, northern Norway: constraints from potential field data, on-land structural mapping and palaeomagnetic data, *Norsk Geologisk Tidsskrift,* **77,** 15–33.

Olesen, O. *et al.*, 2002. Bridging the gap between the Nordland onshore and offshore geology, *Norwegian J. Geol.,* **82,** 243–262.

Olesen, O. *et al.*, 2007. KONTIKI Final Report, CONTInental Crust and Heat Generation In 3D, *NGU Report 2007.042,* NGU, Geological Survey of Norway.

Olesen, O. *et al.*, 2010. New aeromagnetic and gravity compilations from Norway and adjacent areas: methods and applications, *Geological Society, London, Petroleum Geology Conference Series,* **7,** 559–586.

Olesen, O., Kierulf, H.P., Brönner, M., Dalsegg, E., Fredin, O. & Solbakk, T., 2013. Deep weathering, neotectonics and strandflat formation in Nordland, northern Norway, *Norwegian J. Geol.,* **93,** 189–213.

Osmundsen, P., Sommaruga, A., Skilbrei, J. & Olesen, O., 2002. Deep structure of the mid-Norway rifted margin, *Norwegian J. Geol.,* **82,** 205–224.

Park, R.G., 1992. Plate kinematic history of Baltic during the Middle to Late Proterozoic: a model, *Geology,* **20,** 725–728.

Pascal, C., Ebbing, J. & Skilbrei, J., 2007. Interplay between the Scandes and the Trans-Scandinavian Igneous Belt: integrated thermo-rheological and potential field modelling of the Central Scandes profile, *Norwegian J. Geol.,* **87,** 3–12.

Patchett, P., Todt, W. & Gorbatschev, R., 1987. Origin of continental crust of 1.9–1.7 Ga age; Nd isotopes in the Svecofennian orogenic terrains of Sweden, *Precambrian Res.,* **35,** 145–160.

Pavlis, N.K., Holmes, S.A., Kenyon, S.C. & Factor, J.K., 2008. *An Earth Gravitational Model to Degree 2160: EGM 2008* presented at Session G3: GRACE Science Applications, EGU, Vienna.

Pavlis, N.K., Holmes, S.A., Kenyon, S.C. & Factor, J.K., 2012. The development and evaluation of the Earth Gravitational Model 2008 (EGM2008), *J. geophys. Res.,* **117**(B4), doi:10.1029/2011JB008916.

Pérez-Gussinyé, M., Lowry, A.R., Watts, A.B. & Velicogna, I., 2004. On the recovery of effective elastic thickness using spectral methods: examples from synthetic data and from the Fennoscandian Shield, *J. geophys. Res.,* **109**, B10409, doi:10.1029/2003JB002788.

Plomerová, J., Babuška, V., Vecsey, L. & Kouba, D., 2002. Seismic anisotropy of the lithosphere around the Trans-European Suture Zone (TESZ) based on teleseismic body-wave data of the TOR experiment, *Tectonophysics,* **360**(1–4), 89–114.

Plomerová, J., Babuška, V., Kozlovskaya, E., Vecsey, L. & Hyvönen, L., 2008. Seismic anisotropy - A key to resolve fabrics of mantle lithosphere of Fennoscandia, *Tectonophysics,* **462**(1–4), 125–136.

Rickers, F., Fichtner, A. & Trampert, J., 2013. The Iceland-Jan Mayen plume system and its impact on mantle dynamics in the North Atlantic region: Evidence from full-waveform inversion, *Earth planet. Sci. Lett.,* **367**(0), 39–51.

Riis, F., 1996. Quantification of Cenozoic vertical movements of Scandinavia by correlation of morphological surfaces with offshore data, *Glob. Planet. Change,* **12**(1–4), 331–357.

Seton, M. *et al.*, 2012. Global continental and ocean basin reconstructions since 200 Ma, *Earth-Sci. Rev.,* **113**(3–4), 212–270.

Shomali, Z.H., Roberts, R.G. & the TOR Working Group, 2002, Non-linear body wave teleseismic tomography along the TOR array, *Geophys. J. Int.,* **148**(3), 562–574.

Shomali, Z.H., Roberts, R.G. & Pedersen, L.B., 2006. Lithospheric structure of the Tornquist Zone resolved by nonlinear P and S teleseismic tomography along the TOR array, *Tectonophysics,* **416**(1–4), 133–149.

Skilbrei, J., Olesen, O., Osmundsen, P., Kihle, O., Aaro, S. & Fjellanger, E., 2002. A study of basement structures and onshore-offshore correlations in Central Norway, *Norwegian J. Geol.,* **82,** 263–279.

Slagstad, T., 2008. Radiogenic heat production of Archaean to Permian geological provinces in Norway, *Norwegian J. Geol.,* **88,** 149–166.

Slagstad, T., Balling, N., Elvebakk, H., Midttømme, K., Olesen, O., Olsen, L. & Pascal, C., 2009. Heat-flow measurements in Late Palaeoproterozoic to Permian geological provinces in south and central Norway and a new heat-flow map of Fennoscandia and the Norwegian-Greenland Sea, *Tectonophysics,* **473**(3–4), 341–361.

Smith, W.H.F. & Sandwell, D.T., 1997. Global sea floor topography from satellite altimetry and ship depth soundings, *Science,* **277**(5334), 1956–1962.

Steiger, R.H., Harnik-Šoptrajanova, G., Zimmermann, T. & Henriksen, N., 1976. Isotopic age and metamorphic history of the banded gneiss at Danmarkshavn, East Greenland, *Contrib. Mineral. Petrol.,* **57**(1), 1–24.

Stixrude, L. & Lithgow-Bertelloni, C., 2005. Mineralogy and elasticity of the oceanic upper mantle: Origin of the low-velocity zone, *J. geophys. Res.,* **110**, B03204, doi:10.1029/2004JB002965.

Stratford, W., Thybo, H., Faleide, J.I., Olesen, O. & Tryggvason, A., 2009. New Moho map for onshore southern Norway, *Geophys. J. Int.,* **178**(3), 1755–1765.

Svenningsen, L., Balling, N., Jacobsen, B.H., Kind, R., Wylegalla, K. & Schweitzer, J., 2007. Crustal root beneath the highlands of southern Norway resolved by teleseismic receiver functions, *Geophys. J. Int.,* **170**(3), 1129–1138.

Yuan, H. & Romanowicz, B., 2010. Lithospheric layering in the North American Craton, *Nature,* **466**(7310), 1063–1068.

Zhao, G., Cawood, P.A., Wilde, S.A. & Sun, M., 2002. Review of global 2.1-1.8 Ga orogens: implications for a pre-Rodinia supercontinent, *Earth-Sci. Rev.,* **59**(1–4), 125–162.